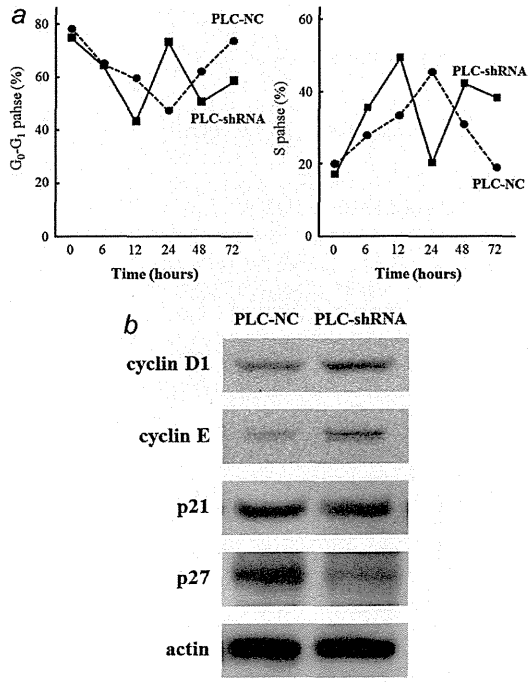

Figure 3. Cell cycle progression assessed by a flow cytometric analysis and the expression of cell cycle-related molecules. (*a*) Time with minimum percentage of G_0/G_1 phase (Left panel) and maximum percentage of S phase (Right panel) was 24 hr and 12 hr in the control cells and the IGFBP7-suppressed cells, respectively. (*b*) Cyclin D1 and cyclin E were increased and p27 was decreased in the IGFBP7-suppressed cells than the control cells, and there was no significant difference in p21 expression between the 2 cells.

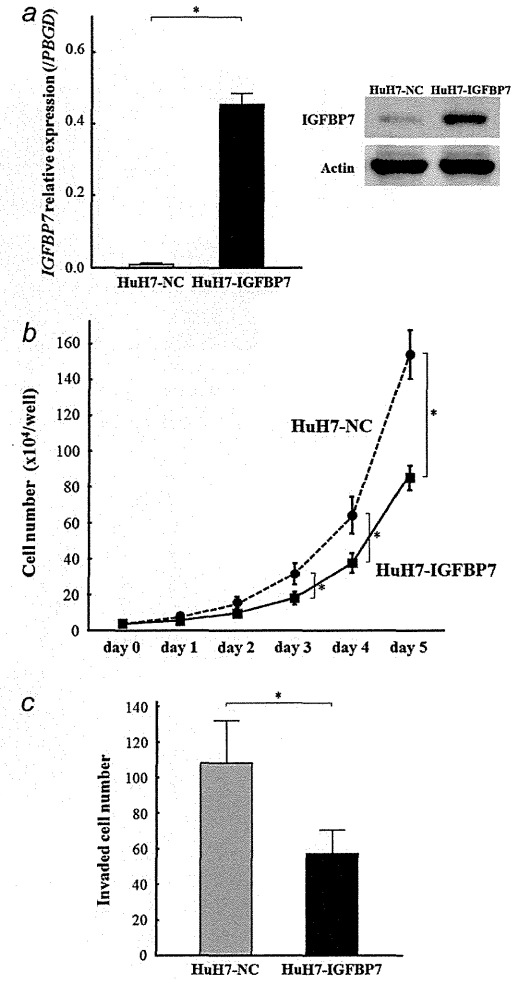

Figure 4. Characteristics of HuH7 transfected with *IGFBP7* expression plasmid. (*a*) qRT-PCR (Left panel) and western blot analysis (Right panel) indicated a significant increase in IGFBP7 in cells transfected with *IGFBP7* expression plasmid compared with control cells (*$p < 0.05$). (*b*) Proliferation assays showed significantly slower growth in the IGFBP7-overexpressing cells compared to the control cells (*$p < 0.05$). (*c*) The invasion assay showed that the invasive ability of the IGFBP7-overexpressing cells was significantly weaker than that of the control cells (*$p < 0.05$). Data are mean ± SD of 3 experiments.

the transfection, as confirmed by qRT-PCR and western blot analysis (Fig. 4*a*). The proliferation assay showed significantly less rapid growth in the IGFBP7-overexpressing cells compared to the control cells (Fig. 4*b*). In addition, the invasive ability of the IGFBP7-overexpressing cells was significantly weaker than that of the control cells (Fig. 4*c*), which were consistent to the results of the above shRNA plasmid experiments.

In vivo studies

IGFBP7 expression correlates with tumor-related factors in clinical HCC samples.. Next, IGFBP7 expression in the tumoral leison was evaluated in clinical sample by immunohistochemical staining. The immunohistochemical analysis showed that among the 104 patients examined, 67 patients (64.4%) showed positive staining for IGFBP7 and the remaining 37 patients (35.6%) were negative for IGFBP7. The immunohistochemical findings of representative cases are shown in Figure 5*a*. The clinicopathological factors related to IGFBP7 expression status of the 104 patients are summarized in Table 1. The data indicated that IGFBP7 expression was significantly associated with maximum tumor size and vascular invasion ($p < 0.0001$, $p = 0.0095$, respectively).

On the other hand, the IGFBP7 expression in nontumoral lesion was homogenously observed in the cytoplasm of cells in all the 104 patients. The immunohistochemically

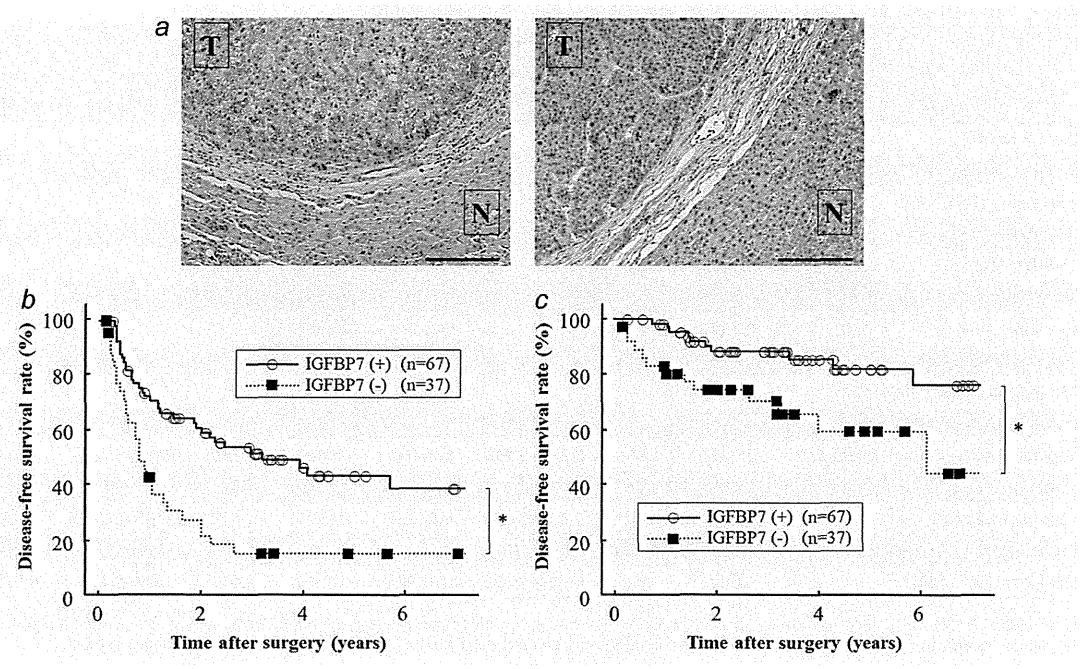

Figure 5. IGFBP7 expression and postoperative outcome in HCC patients. (*a*) Immunohistochemical findings in representative positive case (Left panel) and negative case (Right panel). T, tumoral lesion; N, non-tumoral lesion. Bar = 200 μm. Disease-free survival (*b*) and overall survival (*c*) in patients negative for IGFBP7 expression were significantly poorer than in cells expressing IGFBP7 (*$p < 0.05$).

Table 1. Clinicopathological characteristics of patients with HCC according to IGFBP7 status

	IFGFBP7 (+) ($n = 67$)	IGFBP7 (−) ($n = 37$)	*p*-value
Clinical factors			
Gender (male/female)	53/14	29/8	0.9308
Age (years)[1]	65 ± 10	63 ± 10	0.3900
HBs-Ag (−/+)	52/15	30/7	0.6783
Anti-HCV Ab (−/+)	29/38	15/22	0.7863
Child-Pugh classification (A/B)	58/9	29/8	0.2796
Liver cirrhosis (−/+)	31/36	20/17	0.4470
Tumor-related factors			
AFP (ng/ml)[1]	15,155 ± 122,143	30,243 ± 86,058	0.5075
PIVKA-II (mAU/ml)[1]	26,656 ± 87,446	151,639 ± 1,221,431	0.5365
Number of tumors (single/multiple)	47/20	21/16	0.1693
Maximum tumor size (cm)	3.2 ± 1.7	6.5 ± 4.7	<0.0001
Vascular invasion (−/+)	58/9	24/13	0.0095
Edmondson-Steiner grade (I,II/III,IV)	31/36	11/26	0.0998

[1]Data are expressed as mean ± SD.
Abbreviations: IGFBP7, insulin-like growth factor binding protein 7; HBs-Ag, hepatitis B surface antigen; Anti-HCV Ab, anti-hepatic C virus antibody; AFP:, alpha-fetoprotein; PIVKA-II, protein induced by vitamin K absence or antagonists-II.

determined IGFBP7 expression level was similar between 53 cirrhotic patients and the remaining 51 non-cirrhotic patients.

IGFBP7 downregulation is an independent significant predictor for postoperative outcome in HCC patients. The disease-free survival (DFS) in patients without IGFBP7 expression (1-/

Table 2. Statistical analysis of disease-free survival and overall survival of patients with HCC

	Disease-free survival				Overall survival			
	Univariate	Multivariate			Univariate	Multivariate		
	p-value	OR	95% CI	*p*-value	*p*-value	OR	95% CI	*p*-value
Clinical factors								
Gender (male/female)	0.2192				0.1968			
Age (years) (≤64/>64)	0.5542				0.8018			
HBs-Ag (−/+)	0.2440				0.3605			
Anti-HCV Ab (−/+)	0.9405				0.5034			
Child-Pugh classification (A/B)	0.2586				0.7501			
Liver cirrhosis (−/+)	0.1429				0.5587			
Tumor-related factors								
AFP (ng/ml) (≤400/>400)	0.0629				0.1042			
PIVKA-II (mAU/ml) (≤40/>40)	0.2912				0.1563			
Number of tumors (single/multiple)	0.0025	1.659	0.978–2.815	0.0604	0.0007	2.288	0.905–5.780	0.0801
Maximum tumor size (cm) (≤5/>5)	0.0001	1.387	0.737–2.611	0.3100	0.0290	1.512	0.579–3.949	0.3991
Vascular invasion (−/+)	<0.0001	2.681	1.400–5.135	0.0029	<0.0001	4.649	1.705–12.679	0.0027
Edmondson-Steiner grade (I,II/III,IV)	0.0392	1.520	0.894–2.574	0.1225	0.0180	5.587	1.616–19.231	0.0066
IGFBP7 status (−/+)	0.0007	1.919	1.112–3.313	0.0192	0.0063	2.659	1.102–6.418	0.0296

Abbreviations: IGFBP7, insulin-like growth factor binding protein 7; HBs-Ag, hepatitis B surface antigen; Anti-HCV Ab, anti-hepatic C virus antibody; AFP:, alpha-fetoprotein; PIVKA-II, protein induced by vitamin K absence or antagonists-II; OR, odds ratio; 95% CI, 95% confidence interval.

3-/5-year: 42.9%/15.3%/15.3%) was significantly poorer than that in patients showing IGFBP7 expression (1-/3-/5-year: 70.9%/51.8%/43.6%) ($p = 0.0002$; Fig. 5*b*). Univariate analyses showed that number of tumors ($p = 0.0025$), maximum tumor size ($p = 0.0001$), presence/absence of vascular invasion ($p < 0.0001$), and Edmondson-Steiner grade ($p = 0.0392$) all significantly correlated with DFS, in addition to IGFBP7 status (Table 2). Multivariate analysis for DFS using the above 5 factors identified presence/absence of vascular invasion and IGFBP7 status as independent significant factors (Table 2).

The overall survival (OS) rate in patients without IGFBP7 expression (1-/3-/5-year: 83.4%/70.2%/59.2%) was also significantly lower than that in patients with positive IGFBP7 expression (1-/3-/5-year: 98.5%/88.4%/82.0%) ($p = 0.0063$; Fig. 5*c*). By univariate analysis, number of tumors ($p = 0.0007$), maximum tumor size ($p = 0.0290$), presence/absence of vascular invasion ($p < 0.0001$), and Edmondson-Steiner grade ($p = 0.0180$) were also significantly correlated with OS (Table 2). Multivariate analysis using the above 5 factors identified presence/absence of vascular invasion, Edmondson-Steiner grade, and IGFBP7 status as independent significant factors in OS (Table 2). Thus, IGFBP7 expression was an overall independent significant factor for postoperative prognosis in HCC patients.

Discussion

In this study, we first analyzed IGFBP7 function *in vitro* experiments. The results demonstrated that IGFBP7 downregulation was significantly associated with rapid growth and proliferation of HCC cells. In addition, the cells showed decreased apoptotic cell numbers and expression of apoptosis-related proteins, enhancement of ERK signaling, and rapid cell cycle progression. Considering the implicated tumor suppression activity of IGFBP7, the results of this study are consistent with previous similar reports.[7,9–11,14,15,21] We also previously reported a significant association of IGFBP7 downregulation with resistance to some chemotherapeutic drugs in HCC cells.[17] Taken together, it seems apparent that IGFBP7 downregulation is significantly associated with the malignant potential of cancer cells including proliferation, invasiveness, and resistance to chemotherapeutic drugs. To our knowledge, this is the first study to examine the functional role of IGFBP7 in HCC. On the other hand, the cause-and-effect relationship between the IGFBP7 downregulation and the malignant potential is still unsolved, which is expected to be elucidated by further studies in future.

This study also assessed the prognostic significance of IGFBP7 expression in resected human HCC samples. From these findings, IGFBP7 downregulation was significantly associated with tumor progression and postoperative poor prognosis in our patients group, and IGFBP7 status was identified as an independent significant prognostic factor, in addition to other well-known factors. This finding was consistent with the results of the *in vitro* experiments and serves to suggest that assessing the IGFBP7 expression status of patients with HCC could improve the prediction of prognosis.

We have reported some studies of significant prognostic predictors after surgery for HCC.[20,23–38] In one of the studies, based on cDNA microarray analysis, we identified a set of multiple genes whose expressions were significantly different

between patients with good prognosis and those with poor prognosis, and revealed that the gene set was one of the independent prognostic factors.[38] IGFBP7 was not included in the gene set because the difference of the expression level was not large between the 2 groups, but the IGFBP7 expression level examined by the microarray analysis was also significantly correlated to the prognosis. This result seems to be consistent with the result of this study. In addition, considering the significant inverse correlation of IGFBP7 expression to the extent of apoptosis and cell cycle progression confirmed by the *in vitro* experiments, our previous reports of apoptosis- and cell cycle-related molecules as prognostic factors are in agreement with the prognostic impact of IGFBP7.[25,26,34,35] Furthermore, we have reported that angiogenesis-related molecules such as angiopoietin-2 and hypoxia-induced factor-1α are significant factors for postoperative prognosis.[33] Considering that IGFBP7 was reported to block angiogenesis in human vascular endothelial cells, it may be possible that there is a significant correlation between IGFBP7 expression and the angiogenesis-related molecules, though we did not examine it in this study.[39]

IGFBP7 is a secreted protein, and recombinant IGFBP7 is commonly purified.[40,41] Indeed, previous studies of IGFBP7 function have expressed the protein exogenously using IGFBP7 viral vectors or by administering recombinant protein.[39] In addition, IGFBP7 has also been studied as a possible therapeutic agent for treatment of malignancies that are dependent on BRAF-MEK-ERK signaling.[10,42] Thus, recombinant IGFBP7 could be potentially suitable therapeutically to improve the poor prognosis of HCC patients lacking IGFBP7 expression. In addition, IGFBP7 expression is also subject to epigenetic modification, and aberrant methylation of CpG islands in the *IGFBP7* promoter region was confirmed in several kinds of cancers.[10,43] In this regard, Wajapeyee *et al.*[10] showed that treatment of melanoma cell lines with DNA methyltransferase inhibitor, 5-aza-2′-deoxycytidine, restored IGFBP7 expression. Such a finding suggests a therapeutic application whereby IGFBP7 expression and thus function are restored using a DNA methyltransferase inhibitor. Exploring these therapeutic interventions against HCC was unfortunately beyond the scope of this study, and further studies are definitely needed in this regard.

In summary, we found that IGFBP7 downregulation was significantly associated with both tumor progression and clinical outcome in HCC. This result suggested that analysis of IGFBP7 expression in patients might help to predict prognosis, and that IGFBP7 could be a novel therapeutic target in HCC patients with poor prognosis.

References

1. Block TM, Mehta AS, Fimmel CJ, Jordan R. Molecular viral oncology of hepatocellular carcinoma. *Oncogene* 2003; 22:5093–107.
2. Bosch FX, Ribes J, Diaz M, Cleries R. Primary liver cancer: worldwide incidence and trends. *Gastroenterology* 2004;127: S5–S16.
3. Zhu AX. Systemic therapy of advanced hepatocellular carcinoma: how hopeful should we be? *Oncologist* 2006;11:790–800.
4. Tung-Ping Poon R, Fan ST, Wong J. Risk factors, prevention, and management of postoperative recurrence after resection of hepatocellular carcinoma. *Ann Surg* 2000; 232:10–24.
5. Zhao WH, Ma ZM, Zhou XR, Feng YZ, Fang BS. Prediction of recurrence and prognosis in patients with hepatocellular carcinoma after resection by use of CLIP score. *World J Gastroenterol* 2002;8:237–42.
6. Zhou J, Tang ZY, Wu ZQ, Zhou XD, Ma ZC, Tan CJ, Shi YH, Yu Y, Qiu SJ, Fan J. Factors influencing survival in hepatocellular carcinoma patients with macroscopic portal vein tumor thrombosis after surgery, with special reference to time dependency: a single-center experience of 381 cases. *Hepatogastroenterology* 2006;53: 275–80.
7. Mutaguchi K, Yasumoto H, Mita K, Matsubara A, Shiina H, Igawa M, Dahiya R, Usui T. Restoration of insulin-like growth factor binding protein-related protein 1 has a tumor-suppressive activity through induction of apoptosis in human prostate cancer. *Cancer Res* 2003;63: 7717–23.
8. Sato Y, Chen Z, Miyazaki K. Strong suppression of tumor growth by insulin-like growth factor-binding protein-related protein 1/tumor-derived cell adhesion factor/mac25. *Cancer Sci* 2007;98:1055–63.
9. Kato MV. A secreted tumor-suppressor, mac25, with activin-binding activity. *Mol Med* 2000;6:126–35.
10. Wajapeyee N, Serra RW, Zhu X, Mahalingam M, Green MR. Oncogenic BRAF induces senescence and apoptosis through pathways mediated by the secreted protein IGFBP7. *Cell* 2008;132:363–74.
11. Wilson HM, Birnbaum RS, Poot M, Quinn LS, Swisshelm K. Insulin-like growth factor binding protein-related protein 1 inhibits proliferation of MCF-7 breast cancer cells via a senescence-like mechanism. *Cell Growth Differ* 2002;13:205–13.
12. Lin J, Lai M, Huang Q, Ruan W, Ma Y, Cui J. Reactivation of IGFBP7 by DNA demethylation inhibits human colon cancer cell growth in vitro. *Cancer Biol Ther* 2008; 7:1896–900.
13. Burger AM, Zhang X, Li H, Ostrowski JL, Beatty B, Venanzoni M, Papas T, Seth A. Down-regulation of T1A12/mac25, a novel insulin-like growth factor binding protein related gene, is associated with disease progression in breast carcinomas. *Oncogene* 1998;16:2459–67.
14. Landberg G, Ostlund H, Nielsen NH, Roos G, Emdin S, Burger AM, Seth A. Downregulation of the potential suppressor gene IGFBP-rP1 in human breast cancer is associated with inactivation of the retinoblastoma protein, cyclin E overexpression and increased proliferation in estrogen receptor negative tumors. *Oncogene* 2001;20:3497–505.
15. Ruan WJ, Lin J, Xu EP, Xu FY, Ma Y, Deng H, Huang Q, Lv BJ, Hu H, Cui J, Di MJ, Dong JK, et al. IGFBP7 plays a potential tumor suppressor role against colorectal carcinogenesis with its expression associated with DNA hypomethylation of exon 1. *J Zhejiang Univ Sci B* 2006;7:929–32.
16. Kondo M, Nagano H, Wada H, Damdinsuren B, Yamamoto H, Hiraoka N, Eguchi H, Miyamoto A, Yamamoto T, Ota H, Nakamura M, Marubashi S, et al. Combination of IFN-alpha and 5-fluorouracil induces apoptosis through IFN-alpha/beta receptor in human hepatocellular carcinoma cells. *Clin Cancer Res* 2005;11:1277–86.
17. Tomimaru Y, Eguchi H, Wada H, Noda T, Murakami M, Kobayashi S, Marubashi S, Takeda Y, Tanemura M, Umeshita K, Doki Y, Mori M, et al. Insulin-like growth

factor-binding protein 7 alters the sensitivity to interferon-based anticancer therapy in hepatocellular carcinoma cells. *Br J Cancer* 2010;102:1483–90.
18. Nakamura M, Nagano H, Sakon M, Yamamoto T, Ota H, Wada H, Damdinsuren B, Noda T, Marubashi S, Miyamoto A, Takeda Y, Umeshita K, et al. Role of the Fas/FasL pathway in combination therapy with interferon-alpha and fluorouracil against hepatocellular carcinoma in vitro. *J Hepatol* 2007;46:77–88.
19. Eguchi H, Nagano H, Yamamoto H, Miyamoto A, Kondo M, Dono K, Nakamori S, Umeshita K, Sakon M, Monden M. Augmentation of antitumor activity of 5-fluorouracil by interferon alpha is associated with up-regulation of p27Kip1 in human hepatocellular carcinoma cells. *Clin Cancer Res* 2000;6: 2881–90.
20. Kondo M, Yamamoto H, Nagano H, Okami J, Ito Y, Shimizu J, Eguchi H, Miyamoto A, Dono K, Umeshita K, Matsuura N, Wakasa K, et al. Increased expression of COX-2 in nontumor liver tissue is associated with shorter disease-free survival in patients with hepatocellular carcinoma. *Clin Cancer Res* 1999;5:4005–12.
21. Vizioli MG, Sensi M, Miranda C, Cleris L, Formelli F, Anania MC, Pierotti MA, Greco A. IGFBP7: an oncosuppressor gene in thyroid carcinogenesis. *Oncogene* 2010; 29:3835–44.
22. Lugli E, Troiano L, Ferraresi R, Roat E, Prada N, Nasi M, Pinti M, Cooper EL, Cossarizza A. Characterization of cells with different mitochondrial membrane potential during apoptosis. *Cytometry A* 2005;68:28–35.
23. Arai I, Nagano H, Kondo M, Yamamoto H, Hiraoka N, Sugita Y, Ota H, Yoshioka S, Nakamura M, Wada H, Damdinsuren B, Kato H, et al. Overexpression of MT3-MMP in hepatocellular carcinoma correlates with capsular invasion. *Hepatogastroenterology* 2007;54:167–71.
24. Damdinsuren B, Nagano H, Kondo M, Yamamoto H, Hiraoka N, Yamamoto T, Marubashi S, Miyamoto A, Umeshita K, Dono K, Nakamori S, Wakasa K, et al. Expression of Id proteins in human hepatocellular carcinoma: relevance to tumor dedifferentiation. *Int J Oncol* 2005; 26:319–27.
25. Ito Y, Matsuura N, Sakon M, Miyoshi E, Noda K, Takeda T, Umeshita K, Nagano H, Nakamori S, Dono K, Tsujimoto M, Nakahara M, et al. Expression and prognostic roles of the G1-S modulators in hepatocellular carcinoma: p27 independently predicts the recurrence. *Hepatology* 1999;30:90–9.
26. Ito Y, Matsuura N, Sakon M, Takeda T, Umeshita K, Nagano H, Nakamori S, Dono K, Tsujimoto M, Nakahara M, Nakao K, Monden M. Both cell proliferation and apoptosis significantly predict shortened disease-free survival in hepatocellular carcinoma. *Br J Cancer* 1999;81:747–51.
27. Kittaka N, Takemasa I, Seno S, Takeda Y, Kobayashi S, Marubashi S, Dono K, Umeshita K, Nagano H, Matsuda H, Monden M, Mori M, et al. Exploration of potential genomic portraits associated with intrahepatic recurrence in human hepatocellular carcinoma. *Ann Surg Oncol* 2010;17:3145–54.
28. Kittaka N, Takemasa I, Takeda Y, Marubashi S, Nagano H, Umeshita K, Dono K, Matsubara K, Matsuura N, Monden M. Molecular mapping of human hepatocellular carcinoma provides deeper biological insight from genomic data. *Eur J Cancer* 2008;44:885–97.
29. Miyamoto A, Nagano H, Sakon M, Fujiwara Y, Sugita Y, Eguchi H, Kondo M, Arai I, Morimoto O, Dono K, Umeshita K, Nakamori S, et al. Clinical application of quantitative analysis for detection of hematogenous spread of hepatocellular carcinoma by real-time PCR. *Int J Oncol* 2001;18:527–32.
30. Morimoto O, Nagano H, Sakon M, Fujiwara Y, Yamada T, Nakagawa H, Miyamoto A, Kondo M, Arai I, Yamamoto T, Ota H, Dono K, et al. Diagnosis of intrahepatic metastasis and multicentric carcinogenesis by microsatellite loss of heterozygosity in patients with multiple and recurrent hepatocellular carcinomas. *J Hepatol* 2003;39:215–21.
31. Noda T, Nagano H, Tomimaru Y, Murakami M, Wada H, Kobayashi S, Marubashi S, Eguchi H, Takeda Y, Tanemura M, Umeshita K, Kim T, et al. Prognosis of hepatocellular carcinoma with biliary tumor thrombi following liver surgery. *Surgery* 2011;149:371–7.
32. Sakon M, Umeshita K, Nagano H, Eguchi H, Kishimoto S, Miyamoto A, Ohshima S, Dono K, Nakamori S, Gotoh M, Monden M. Clinical significance of hepatic resection in hepatocellular carcinoma: analysis by disease-free survival curves. *Arch Surg* 2000;135:1456–9.
33. Wada H, Nagano H, Yamamoto H, Yang Y, Kondo M, Ota H, Nakamura M, Yoshioka S, Kato H, Damdinsuren B, Tang D, Marubashi S, et al. Expression pattern of angiogenic factors and prognosis after hepatic resection in hepatocellular carcinoma: importance of angiopoietin-2 and hypoxia-induced factor-1 alpha. *Liver Int* 2006;26:414–23.
34. Xu X, Yamamoto H, Sakon M, Yasui M, Ngan CY, Fukunaga H, Morita T, Ogawa M, Nagano H, Nakamori S, Sekimoto M, Matsuura N, et al. Overexpression of CDC25A phosphatase is associated with hypergrowth activity and poor prognosis of human hepatocellular carcinomas. *Clin Cancer Res* 2003;9:1764–72.
35. Xu X, Sakon M, Nagano H, Hiraoka N, Yamamoto H, Hayashi N, Dono K, Nakamori S, Umeshita K, Ito Y, Matsuura N, Monden M. Akt2 expression correlates with prognosis of human hepatocellular carcinoma. *Oncol Rep* 2004; 11:25–32.
36. Yamamoto S, Tomita Y, Nakamori S, Hoshida Y, Nagano H, Dono K, Umeshita K, Sakon M, Monden M, Aozasa K. Elevated expression of valosin-containing protein (p97) in hepatocellular carcinoma is correlated with increased incidence of tumor recurrence. *J Clin Oncol* 2003;21: 447–52.
37. Yang Y, Nagano H, Ota H, Morimoto O, Nakamura M, Wada H, Noda T, Damdinsuren B, Marubashi S, Miyamoto A, Takeda Y, Dono K, et al. Patterns and clinicopathologic features of extrahepatic recurrence of hepatocellular carcinoma after curative resection. *Surgery* 2007;141: 196–202.
38. Yoshioka S, Takemasa I, Nagano H, Kittaka N, Noda T, Wada H, Kobayashi S, Marubashi S, Takeda Y, Umeshita K, Dono K, Matsubara K, et al. Molecular prediction of early recurrence after resection of hepatocellular carcinoma. *Eur J Cancer* 2009;45:881–9.
39. Tamura K, Hashimoto K, Suzuki K, Yoshie M, Kutsukake M, Sakurai T. Insulin-like growth factor binding protein-7 (IGFBP7) blocks vascular endothelial cell growth factor (VEGF)-induced angiogenesis in human vascular endothelial cells. *Eur J Pharmacol* 2009;610:61–7.
40. Akaogi K, Okabe Y, Sato J, Nagashima Y, Yasumitsu H, Sugahara K, Miyazaki K. Specific accumulation of tumor-derived adhesion factor in tumor blood vessels and in capillary tube-like structures of cultured vascular endothelial cells. *Proc Natl Acad Sci USA* 1996;93:8384–9.
41. Oh Y, Nagalla SR, Yamanaka Y, Kim HS, Wilson E, Rosenfeld RG. Synthesis and characterization of insulin-like growth factor-binding protein (IGFBP)-7. Recombinant human mac25 protein specifically binds. IGF-I and -II. *J Biol Chem* 1996;271:30322–5.
42. Wajapeyee N, Kapoor V, Mahalingam M, Green MR. Efficacy of IGFBP7 for treatment of metastatic melanoma and other cancers in mouse models and human cell lines. *Mol Cancer Ther* 2009;8:3009–14.
43. Lin J, Lai M, Huang Q, Ma Y, Cui J, Ruan W. Methylation patterns of IGFBP7 in colon cancer cell lines are associated with levels of gene expression. *J Pathol* 2007; 212:83–90.

J Gastroenterol
DOI 10.1007/s00535-011-0511-x

RAPID COMMUNICATION

Early evaluation of transcatheter arterial chemoembolization-refractory hepatocellular carcinoma

Kenya Yamanaka · Etsuro Hatano · Koji Kitamura · Taku Iida · Takamichi Ishii · Takahumi Machimito · Kojiro Taura · Kentaro Yasuchika · Hiroyoshi Isoda · Toshiya Shibata · Shinji Uemoto

Received: 31 May 2011 / Accepted: 14 November 2011

Abstract
Background There is no standard therapy for patients with transcatheter arterial chemoembolization (TACE)-refractory hepatocellular carcinoma (HCC). This study examined whether evaluating the tumor effect (TE) at 1 week after TACE was useful for predicting refractoriness to TACE.
Methods We performed a historical cohort study involving 54 patients and 119 tumors. TE was evaluated at 1 week and 3 months after TACE, and an overall evaluation was also performed at 3 months based on the response evaluation criteria in cancer of the liver.
Results Among 45 tumors evaluated as TE2 at 1 week, 43 tumors (95.6%) were classified as TE1 or TE2 at 3 months. Of the 24 patients whose tumors were categorized as TE2 at 1 week, none achieved a complete or partial response.
Conclusions Evaluating the TE at 1 week after TACE is useful for the early diagnosis of TACE-refractory HCC and allows alternative treatment options, such as sorafenib, to be employed before the disease progresses.

Keywords Hepatocellular carcinoma · Transcatheter arterial chemoembolization · Tumor effects

K. Yamanaka · E. Hatano (✉) · K. Kitamura · T. Iida · T. Ishii · T. Machimito · K. Taura · K. Yasuchika · S. Uemoto
Department of Surgery, Graduate School of Medicine, Kyoto University, 54 Kawaharacho, Shogoin, Sakyo-ku, Kyoto 606-8507, Japan
e-mail: etsu@kuhp.kyoto-u.ac.jp

H. Isoda · T. Shibata
Department of Diagnostic Imaging and Nuclear Medicine, Graduate School of Medicine, Kyoto University, Kyoto, Japan

Introduction

Transcatheter arterial chemoembolization (TACE) provides a survival benefit in patients with unresectable or relapsed hepatocellular carcinoma (HCC) [1]. TACE is recommended for HCC patients who have been categorized as A or B on the Child–Pugh classification [2]. The selection criteria for TACE are affected by the patient's history of resection, the location of the recurrent HCC, and portal tumor thrombosis. However, repetitive TACE treatments might reduce liver function and induce stenosis of the hepatic artery. Furthermore, even if liver function is preserved in patients whose disease has been defined as Child–Pugh classification A or B, repetitive TACE treatments become less effective in patients with relapsed HCC. These cases are considered TACE-refractory in clinical practice. No effective treatment for TACE-refractory HCC has been established.

Sorafenib is a molecular-targeted agent that is used to prolong the survival of patients with advanced HCC [3, 4]. Recently, it was suggested that sorafenib has beneficial effects on metastatic or TACE-refractory HCC [5]. According to consensus statements from the Japan Society of Hepatology, TACE-refractory HCC patients belonging to Child–Pugh group A are candidates for sorafenib monotherapy as a second-line treatment option [6].

However, refractoriness to TACE is not well defined. Although it is desirable to assess the tumor effect (TE) at least 1 month after TACE, overall response evaluations are performed 3 months after TACE, according to the response evaluation criteria in cancer of the liver (RECICL) [7]. This delay in performing the evaluation is a major concern because of the risk of recurrence and/or tumor progression. If TACE-refractory HCC could be evaluated early, patients with TACE-refractory HCC could be treated with

Published online: 21 December 2011

alternative treatments, such as sorafenib. Therefore, this study examined whether TE evaluations conducted at 1 week after TACE treatment could be used to predict the TE of TACE and the results of the overall response evaluation in order to provide an early diagnosis of TACE refractoriness.

Methods

Study design and eligibility criteria

The Kyoto University Graduate School and Faculty of Medicine Ethics Committee approved this study (E-1071) in accordance with the ethics guidelines for epidemiologic studies in Japan. All patients gave their informed consent for TACE. We performed a historical cohort study to assess the efficacy of TACE. Patients at Kyoto University Hospital who were diagnosed with HCC and treated with TACE between 1 June 2009 and 31 December 2009 were selected for this study. The clinical variables selected in this study were age, sex, hepatitis B surface antigen, hepatitis C virus antibody, history of resection and local ablation therapy, the number of previous TACE treatments, Child–Pugh classification, platelet count, alpha-fetoprotein levels, levels of prothrombin induced by vitamin K absence or antagonist-II, chemotherapeutic agents administered, and the number of tumors. These variables were measured before TACE therapy.

Treatment

Epirubicin® (Nipponkayaku, Tokyo, Japan) dissolved in contrast medium and then suspended in Lipiodol was injected as selectively as possible into the hepatic segmental artery supplying the HCC. Gelfoam® sponges (Pfizer, NY, USA) were used for the embolization. No repeat TACE treatment was scheduled unless the tumor relapsed.

Assessment of efficacy

The efficacy of TACE was assessed by performing dynamic computed tomography (CT; Aquilion TSX-101A, Toshiba Medical Systems, Japan) or magnetic resonance imaging (MRI; MAGNETOM Skyra, Siemens, Germany) before and 3 months after the TACE treatment. For the early evaluation performed 1 week after the TACE, plain CT was performed to assess the uptake of Lipiodol. CT angiography was not routinely performed during TACE. MRI was used for patients that displayed an allergic reaction to the contrast medium and patients who did not demonstrate a typical target lesion on dynamic CT. The tumors targeted in the TE assessment were selected during the CT or MRI conducted before the TACE. The response to TACE was calculated according to RECICL [7]. The tumor-necrotizing effect and tumor size reduction rate were assessed on the basis of the reduction in tumor size or the disappearance of hypervascularity from the nodule using bi-dimensional measurements. The rate of reduction of the necrotic area was estimated from the Lipiodol accumulation observed on CT after TACE. The TE for each targeted tumor was defined as follows: TE4, the disappearance of the tumor or a 100% tumor-necrotizing effect; TE3, a $\geq$50% reduction in tumor size or a $\geq$50% tumor-necrotizing effect; TE1, a $\geq$25% increase in tumor size regardless of the necrotizing effect; and TE2, cases that did not qualify as TE4, TE3, or TE1. The TE determined at 1 week after the TACE treatment was defined as the early TE in this study.

The CT or MR images obtained at 3 months after the TACE treatment were used for the overall evaluation, which was performed according to the RECICL [7]. When there were more than 5 tumors, only 5 tumors were targeted. The overall evaluation was defined using the total tumor load of all the targeted tumors as follows: complete response (CR), disappearance of the tumor or a 100% tumor-necrotizing effect in all tumors; partial response (PR), $\geq$50% reduction in tumor size or a $\geq$50% tumor-necrotizing effect; progressive disease (PD), $\geq$25% increase in tumor size or the emergence of a new tumor; and stable disease (SD), the cases that were not classified as CR, PR, or PD.

Statistical analysis

We examined the relationship between early TE and TE at 3 months. To calculate the sensitivity and specificity of early TE for each tumor, we divided TE into two categories, TE3/4 and TE1/2. Furthermore, we examined the relationship between early TE and the results of the overall evaluation. We also divided the overall evaluation into two categories, CR/PR and SD/PD, to calculate the sensitivity and specificity of early TE. In patients with multiple tumors, we used the lowest TE in our analysis.

Results

Patients

Among the 80 consecutive patients treated with TACE for HCC, the patients who did not undergo any radiological imaging at 3 months after TACE ($n = 10$), who were administered sorafenib ($n = 1$), who underwent TACE with additional percutaneous ethanol injection therapy or radiofrequency ablation ($n = 10$), who underwent TACE

without embolization ($n = 4$), or who underwent TACE using cisplatin instead of epirubicin ($n = 1$) were excluded from this study. Thus, 54 patients with 119 tumors were enrolled in this study. The characteristics of the patients are shown in Table 1.

Relationship between early TE and TE at 3 months after TACE

Early TE1, early TE2, early TE3, and early TE4 were observed in 0, 45, 34, and 40 tumors, respectively. As for the TE observed at 3 months after TACE, TE1, TE2, TE3, and TE4 were observed in 32, 35, 6, and 46 tumors, respectively (Table 2). The sensitivity and specificity of early TE for predicting the TE at 3 months were 64.2 and 96.2%, respectively. Among the 45 tumors evaluated as early TE2, 19 and 24 tumors were evaluated as TE1 and TE2, respectively, at 3 months after TACE. Thus, the positive predictive value of early TE was 95.6%.

Relationship between early TE and the results of the overall evaluation

In the overall evaluation, CR, PR, SD, and PD were observed in 11, 1, 5, and 37 patients, respectively (Table 3). Compared with the response rate achieved in other studies [8], the CR (22%) and disease control rates (31%) were relevant. The sensitivity and specificity of early TE for predicting the results of the overall evaluation were 57.1 and 100%, respectively. Among the 24 patients whose tumors were evaluated as early TE2, 20 patients were evaluated as PD and 4 patients were categorized as SD. Thus, the positive predictive value of early TE was 100%, suggesting that the designation "early TE2" indicates reduced TACE effectiveness.

Discussion

HCC is staged on the basis of the Barcelona Clinic Liver Cancer (BCLC) staging system, and TACE is considered to be effective for patients with intermediate stage HCC [9]. However, TACE failure or TACE-refractory HCC is often observed after repeated TACE treatments. The response rate for TACE has been reported to be 15–55% [8]. TACE failure is defined by the following circumstances: an inability to select the feeding artery of the HCC because of arterial devastation, a deterioration of liver function due to repeated TACE treatments, and/or tumor thrombosis of the portal vein. TACE refractoriness is defined using four factors: repetitive tumor recurrence in the liver, the appearance of vascular invasion, the appearance of distant metastasis, and a continuous increase in tumor marker levels after TACE. Repetitive recurrence is diagnosed according to the RECICL, which indicate that the assessment should be performed at least 1 month after TACE. Furthermore, a time interval of 2 or 3 months is usually required between TACE treatments. Therefore, the time period between the initial TACE therapy and the next TACE treatment needs to be more than 3 months.

According to a subanalysis performed as part of the sorafenib HCC assessment randomized protocol (SHARP) study [3], it is expected that treatment with sorafenib in combination with TACE will markedly prolong the overall survival of HCC patients [6]. Several clinical trials such as the global sorafenib placebo in combination with TACE (SPACE) trial and the Japanese TACE therapy in combination with sorafenib (TACTICS) trial have been conducted to analyze the effect of combining TACE therapy with sorafenib. However, in a phase III study conducted in Japan and Korea of sorafenib treatment in patients with advanced HCC, who were administered the drug after

Table 1 Patient characteristics

Characteristics		Number of patients (%)
Age	Median (range)	72 (49–84)
Sex	Male	45 (83)
Hepatitis B surface antigen	Positive	6 (11)
Hepatitis C virus antibody	Positive	24 (44)
History of resection		35 (64)
History of local ablation therapy		25 (46)
No. of previous TACEs	Median (range)	2 (0–9)
Child–Pugh classification	A/B	48/6 (89/11)
Platelet count ($\times 10^9$/L)	Median (range)	9.2 (4.4–40)
Alpha-fetoprotein (ng/dL)	Median (range)	14.9 (2.0–9,282)
PIVKA-II (mAU/mL)	Median (range)	61 (11–33,000)
Chemotherapeutic agent	Median (range)	28.5 (10–45)
Tumor diameter (cm)	≤2/>2	38/16 (70/30)
Number of tumors	Single/multiple	21/33 (39/61)

PIVKA-II prothrombin induced by vitamin K absence or antagonist-II, *TACE* transcatheter arterial chemoembolization

Table 2 Relationship between early TE and TE after TACE

Number of tumors	TE (3 months)				Total
	1	2	3	4	
Early TE (1 week)					
2	19	24	2	0	45
3	9	8	3	14	34
4	4	3	1	32	40
Total	32	35	6	46	119

TE tumor effect

Table 3 Relationship between early TE and overall evaluation

Number of patients	Overall evaluation				Total
	PD	SD	PR	CR	
Early TE (1 week)					
2	20	4	0	0	24
3	8	0	1	6	15
4	9	1	0	5	15
Total	37	5	1	11	54

TE tumor effect, *PD* progressive disease, *SD* stable disease, *PR* partial response, *CR* complete response

TACE [10], the time to progression was not significantly prolonged in HCC patients treated with sorafenib. This negative result was considered to have been caused by the increased number of discontinuations and shorter treatment duration that they experienced, as well as the long time period required between TACE treatment and the start of sorafenib therapy (median 9.3 weeks). Additionally, ineffective TACE is considered to induce a neoangiogenic reaction early after TACE [11]. Therefore, treating TACE-refractory HCC patients with sorafenib earlier might have beneficial effects, even in patients with advanced HCC.

There were some limitations to this study. Early TE displayed sensitivities of 64.2 and 57.1% for predicting TE at 3 months and the results of the overall evaluation, respectively. Therefore, early TE was not very accurate at predicting the TE at 3 months and the results of the overall evaluation. However, we think that assessing early TE is useful because it would allow 57.1% of patients to be treated with alternative options earlier. We are currently conducting a prospective trial regarding the effectiveness of the early evaluation of TACE-refractory HCC (UMIN 000005847). Furthermore, an inability to select the feeding artery of a target HCC is one of the causes of TACE failure, although no tumors with extra feeding arteries were detected by angiography after TACE in this cohort. Chemotherapeutic agents such as cisplatin might affect TE [12, 13], although it is unclear whether the selection of chemotherapeutic agents influences the efficacy of embolization [9].

In conclusion, tumors in which an early evaluation classifies the TE as TE2 tend to display a TE of TE1 or TE2 at 3 months after TACE and so a CR or PR will probably not be achieved in these cases. Thus, conducting early evaluations at 1 week after TACE is useful for predicting TACE-refractory HCC. An early diagnosis of TACE-refractory HCC will allow alternative treatment options, such as sorafenib, to be employed before the disease progresses.

Conflict of interest The authors declare that they have no conflict of interest.

References

1. Llovet JM, Real MI, Montana X, Planas R, Coll S, Aponte J, et al. Arterial embolisation or chemoembolisation versus symptomatic treatment in patients with unresectable hepatocellular carcinoma: a randomised controlled trial. Lancet. 2002;359:1734–9.
2. Arii S, Sata M, Sakamoto M, Shimada M, Kumada T, Shiina S, et al. Management of hepatocellular carcinoma: report of consensus meeting in the 45th annual meeting of the Japan Society of Hepatology (2009). Hepatol Res. 2010;40:667–85.
3. Llovet JM, Ricci S, Mazzaferro V, Hilgard P, Gane E, Blanc JF, et al. Sorafenib in advanced hepatocellular carcinoma. N Engl J Med. 2008;359:378–90.
4. Cheng AL, Kang YK, Chen Z, Tsao CJ, Qin S, Kim JS, et al. Efficacy and safety of sorafenib in patients in the Asia-Pacific region with advanced hepatocellular carcinoma: a phase III randomised, double-blind, placebo-controlled trial. Lancet Oncol. 2009;10:25–34.
5. Furuse J. Sorafenib for the treatment of unresectable hepatocellular carcinoma. Biologics. 2008;2:779–88.
6. Kudo M, Ueshima K. Positioning of a molecular-targeted agent, sorafenib, in the treatment algorithm for hepatocellular carcinoma and implication of many complete remission cases in Japan. Oncology. 2010;78:154–66.
7. Kudo M, Kubo S, Takayasu K, Sakamoto M, Tanaka M, Ikai I, et al. Response Evaluation Criteria in Cancer of the Liver (RECICL) proposed by the Liver Cancer Study Group of Japan (2009 Revised Version). Hepatol Res. 2010;40:686–92.
8. Llovet JM, Bruix J. Novel advancements in the management of hepatocellular carcinoma in 2008. J Hepatol. 2008;48:20–37.
9. Bruix J, Sala M, Llovet JM. Chemoembolization for hepatocellular carcinoma. Gastroenterology. 2004;127:179–88.
10. Kudo M, Imanaka K, Chiba N, Nakachi K, Tak W, Takayama T, et al. Phase III study of sorafenib after transarterial chemoembolization in Japanese and Korean patients with unresectable hepatocellular carcinoma. Eur J Cancer. 2011;47:2117–27.
11. Adriana S, Chiara C, Romilda C, Giorgio P, Roberto R, Anna B, et al. Transcatheter arterial chemoembolization (TACE) in hepatocellular carcinoma (HCC): the role of angiogenesis and invasiveness. Am J Gastroenterol. 2008;103:914–21.
12. Yodono H, Matsuo K, Shinohara A. A retrospective comparative study of epirubicin-lipiodol emulsion and cisplatin-lipiodol suspension for use with transcatheter arterial chemoembolization for treatment of hepatocellular carcinoma. Anticancer Drugs. 2011; 22:277–82.
13. Yamanaka K, Hatano E, Narita M, Taura K, Yasuchika K, Nitta T, et al. Comparative study of cisplatin and epirubicin in transcatheter arterial chemoembolization for hepatocellular carcinoma. Hepatol Res. 2011;41:303–9.

Molecular and Cellular Biology

Higher-Order Chromatin Regulation and Differential Gene Expression in the Human Tumor Necrosis Factor/Lymphotoxin Locus in Hepatocellular Carcinoma Cells

Takehisa Watanabe, Ko Ishihara, Akiyuki Hirosue, Sugiko Watanabe, Shinjiro Hino, Hidenori Ojima, Yae Kanai, Yutaka Sasaki and Mitsuyoshi Nakao

Mol. Cell. Biol. **2012, 32(8):1529. DOI: 10.1128/MCB.06478-11.**
Published Ahead of Print 21 February 2012.

MCB
Journals.ASM.org

Higher-Order Chromatin Regulation and Differential Gene Expression in the Human Tumor Necrosis Factor/Lymphotoxin Locus in Hepatocellular Carcinoma Cells

Takehisa Watanabe,[a,b] Ko Ishihara,[c,e] Akiyuki Hirosue,[a] Sugiko Watanabe,[a] Shinjiro Hino,[a] Hidenori Ojima,[d] Yae Kanai,[d] Yutaka Sasaki,[b] and Mitsuyoshi Nakao[a,e]

Department of Medical Cell Biology, Institute of Molecular Embryology and Genetics, and the Global Center of Excellence Cell Fate Regulation Research and Education Unit,[a] Department of Gastroenterology and Hepatology, Graduate School of Medical Sciences,[b] and Priority Organization for Innovation and Excellence,[c] Kumamoto University, Kumamoto, Japan; Division of Molecular Pathology, National Cancer Center Research Institute, Tokyo, Japan[d]; and Core Research for Evolutional Science and Technology (CREST), Japan Science of Technology Agency, Tokyo, Japan[e]

The three-dimensional context of endogenous chromosomal regions may contribute to the regulation of gene clusters by influencing interactions between transcriptional regulatory elements. In this study, we investigated the effects of tumor necrosis factor (TNF) signaling on spatiotemporal enhancer-promoter interactions in the human *tumor necrosis factor* (*TNF*)/*lymphotoxin* (*LT*) gene locus, mediated by CCCTC-binding factor (CTCF)-dependent chromatin insulators. The cytokine genes *LTα*, *TNF*, and *LTβ* are differentially regulated by NF-κB signaling in inflammatory and oncogenic responses. We identified at least four CTCF-enriched sites with enhancer-blocking activities and a TNF-responsive TE2 enhancer in the *TNF/LT* locus. One of the CTCF-enriched sites is located between the early-inducible *LTα/TNF* promoters and the late-inducible *LTβ* promoter. Depletion of CTCF reduced *TNF* expression and accelerated *LTβ* induction. After TNF stimulation, via intrachromosomal dynamics, these insulators mediated interactions between the enhancer and the *LTα/TNF* promoters, followed by interaction with the *LTβ* promoter. These results suggest that insulators mediate the spatiotemporal control of enhancer-promoter associations in the *TNF/LT* gene cluster.

Chromosomal regions harboring different tissue-specific or cellular-state-specific gene clusters may be influenced by long-range regulatory elements and higher-order chromatin organization (45, 53, 60). Recent studies suggest that transcriptional regulatory elements, such as enhancers, promoters, and chromatin insulators, contribute to gene activation and inactivation via genome accessibility and chromosomal interactions (8, 18). Among these, chromatin insulators are boundary elements that partition the genome into chromosomal subregions, probably through their ability to block interactions between enhancers and promoters when positioned between them (enhancer-blocking effect) (7, 17, 41). However, the precise mechanisms responsible for the enhancer-blocking effect and the relationship with long-range chromatin interactions remain unclear (47, 49). The CCCTC-binding factor CTCF is a highly conserved 11-zinc-finger protein that plays crucial roles at insulator sites (44). CTCF is also reported to function in transcriptional activation (62, 73) and repression (16, 36). In the *IGF2/H19* locus, CTCF binds to the differentially methylated region (DMR) of the *H19* gene to form a predicted chromatin loop structure (6, 22, 42). Genome-wide analyses identified the distribution of the putative CTCF-binding sites and their consensus sequences (4, 27, 28, 69). We and other groups recently determined that CTCF is enriched with cohesin in at least 14,000 sites on the human genome (46, 54, 65). CTCF and cohesin cooperatively form compact chromatin loops, leading to the colocalization of gene promoters and their common enhancer in the human *apolipoprotein* gene locus (40). CTCF has been reported to interact with nuclear substructures (71, 72), chromatin remodeling factors (26, 33), RNA polymerase II (10), and CTCF itself (34, 72), as well as undergoing several posttranslational modifications of the protein (12, 29, 37, 70).

Inflammation involves the activation of a highly coordinated gene expression program (43). The tumor necrosis factor (TNF) superfamily members, TNF (initially termed TNF-α), lymphotoxin α (LTα, also termed TNF-β), and lymphotoxin β (LTβ), are major proinflammatory cytokines that mediate inflammatory responses in autocrine/paracrine manners (63). TNF and LTα form homotrimers and act as soluble ligands for the TNF receptor. In contrast, LTβ forms a heterotrimer with LTα and functions as a membrane-bound ligand for the LTβ receptor. In addition to their physiological roles, the aberrant or unbalanced expression of these cytokines is linked to pathological conditions, such as tissue damage/remodeling (38), metabolic diseases (14, 20), and cancer development (19, 23). Hepatic TNF expression is closely related to steatohepatitis (64), and LTβ expression is significantly involved in liver regeneration (3) and hepatocellular carcinomas (HCCs) (23, 67). The *TNF/LT* genes are clustered within the major histocompatibility complex (MHC) class III region on human chromosome 6p21.3, which is the most gene-dense region of the human genome (68). Interestingly, it is reported that NF-κB does not directly interact with the proximal human *TNF* promoter (9, 15, 59) and that NF-κB activation induced by TNF treatment in-

Received 25 October 2011 **Returned for modification** 1 December 2011
Accepted 7 February 2012
Published ahead of print 21 February 2012
Address correspondence to Mitsuyoshi Nakao, mnakao@gpo.kumamoto-u.ac.jp.
Supplemental material for this article may be found at http://mcb.asm.org/.

doi:10.1128/MCB.06478-11

fluences expression of the *TNF/LT* genes, resulting in the amplified inflammatory response (25). Several DNase-hypersensitive sites, generally suggestive of the presence of regulatory elements, have been found in the *TNF/LT* locus (5, 50, 56, 58). However, a transcriptional mechanism and higher-order chromatin regulation in the human *TNF/LT* locus are unknown.

Investigation of the *TNF/LT* locus identified at least four CTCF/cohesin-enriched insulators and a TNF-responsive TE2 enhancer in human hepatic cells. These CTCF-bound sequences possessed enhancer-blocking activities, and one of the insulators was located between the early-inducible *LTα/TNF* promoters and the late-inducible *LTβ* promoter. Chromosome conformation capture (3C) analyses determined that after TNF stimulation, these CTCF-bound insulators initially associated with the TE2 enhancer and the *LTα*, *TNF*, and *LTβ* promoters, followed by a persistent interaction with the TC3 insulator, the TE2 enhancer, and the *LTβ* promoter. These late-phase interactions were consistent with the formation of a place in which the late-inducible *LTβ* gene was transcriptionally active. TNF stimulation thus induces dynamic changes in higher-order chromatin organization of the overall locus, together with differential expression of the *TNF/LT* genes. Based on our findings that insulators mediate the spatiotemporal control of enhancer-promoter interactions, we propose a dynamic chromatin conformation model and enhancer-blocking mechanism mediated by insulators in the *TNF/LT* locus.

MATERIALS AND METHODS

Cell culture. Hep3B, HCT116, and HeLa cells were cultured in a 1:1 mixture of Dulbecco's modified Eagle's minimum essential medium and Ham's F-12 nutrient medium (DMEM/F12; Sigma) supplemented with 10% (vol/vol) fetal bovine serum (FBS). NeHepLxHT cells were cultured in DMEM/F12 supplemented with 10% (vol/vol) FBS, 10^{-7} M dexamethasone, 10^{-7} M insulin, and 50 μg/ml G418. For TNF stimulation, Hep3B and NeHepLxHT cells were treated with recombinant human TNF-α (210-TA; R&D Systems) at concentrations of 5 ng/ml and 0.5 ng/ml, respectively. For inhibition of NF-κB signaling, BAY11-7082 (10 μM) was added to the medium for 1 h before treatment of the cells with TNF for 0.5 or 1 h.

ChIP and quantitative PCR (qPCR) analysis. Hep3B and NeHepLxHT cells were cross-linked with 1% formaldehyde at 37°C for 10 min. Crude cell lysates were sonicated to generate DNA fragments of 200 to 500 bp. Chromatin immunoprecipitation (ChIP) was performed with anti-CTCF (07-729; Millipore), anti-RAD21 (ab992; Abcam), anti-acetylated histone H3 (06-599; Millipore), anti-acetylated histone H4 (06-866; Millipore), anti-p65 (sc-372; Santa Cruz), anti-p300 (sc-585; Santa Cruz), or anti-RNA polymerase II (phosphor-S5) antibodies (ab5131; Abcam) or with control rabbit IgG (sc-2027; Santa Cruz) (26). Cells were cross-linked for an additional 10 min when anti-p65 and anti-p300 antibodies were used.

DNA enrichment in ChIP samples was determined using qPCR analysis with an ABI Prism 7300 system (Applied Biosystems) and SYBR green fluorescence. The threshold was set to cross a point where PCR amplification was linear, and the cycle number required to reach the threshold was recorded and analyzed using the Microsoft Excel software program. PCR was performed using precipitated DNA and the input DNA. Primer sequences are listed in Table S1 in the supplemental material. Other antibodies used were anti-lamin A/C (sc-7292; Santa Cruz).

Electrophoretic mobility shift assay (EMSA). The CTCF protein was synthesized using a coupled *in vitro* transcription/translation reaction with the TNT T7 Quick system (Promega), according to the manufacturer's protocol. For supershift assays, the reaction mixture was combined with 1 μl anti-CTCF antibodies (612148; BD Biosciences) (40). The sequences of the probes were as follows: H19 DMR, 5′-TGG CAC GGA ATT GGT TGT AGT TGT GGA ATC GGA AGT GGC CGC GCG GCG GCA GTG CAG GCT CAC ACA TCA CAG CCC GAG CCC GCC CCA ACT-3; TC1, 5′-TCT CCA GCA CTT CTT GCT CAG GCA GTA CCC AAA GGG GCC GCC TGG GAG CAG CAG AGA CCA GGC CCA AAG CTG CGG GCT TAC AAC AGG TTA GCC ATC CCA-3′; TC2, 5′-AGA CCC TGG TGT CCT CTC TGG CCT TAT TTA CTC CTG GTC CTC TGC CAG CCC TGC CAC CAG ATG GCC TTC TAA CTC CTT GGT TGA AAG GCC CAT CTC ATT C-3′; TC3, 5′-CCC GGT ACA GAG AGC TGC GCA GCG TGA CCG AGC GG CCC TGG GGG TCC CCG CCG CCA GGG GGC GCC CGG CCC CGG TAG CCG ACG AGA CAG TAG AGG-3′; TC4, 5′-CTT CAC CCA GGT CTC TCC AGA GAG CCT CAG GCC GCT GCC TTT ACT TAG TTC TGT GTT CAA TGC CAG AAT GCT GCC TCC TAC AGG AAG TCC ACC TGT ATT GCC CAC ACC TCC T-3′; negative control, 5′-TGG CAA AAA GAA AGG ACA GGG CTG CAA GGA GAG TAC AGA CAT GTG CTG GTG AGT GCA CTG TCT GCA TAG TTA CAC CAG AGC ATC TTA TCA ATC AGA AAC TTA TC-3′.

Luciferase reporter assay. The reporter vector pIHLE consisted of the *luciferase* gene driven by the mouse *H19* promoter (−818 to +6 from the transcription start site), simian virus 40 (SV40) enhancer, and a 1.8-kb AatII-HindIII fragment containing the *H19* DMR insulator. The plasmid pIHLIE was constructed by inserting the 1.8-kb *H19* DMR fragment between the *luciferase* gene and the enhancer. pIHLTE plasmids were constructed by inserting fragments of about 200 bp, including TC1, TC2, TC3, and TC4, between the *luciferase* gene and the enhancer (pIHLTE-1F/1R, -2F/2R, -3F/3R, and -4F/4R, respectively). For pIHLET, TC fragments were inserted downstream of the enhancer in pIHLE (pIHLET-1F/1R, -2F/2R, -3F/3R, and -4F/4R). To prepare pIHLTE with mutations (pIHLTE-1 M, -2 M, -3 M, and -4 M), base substitutions were introduced in CTCF consensus sequences at the TC1, TC2, TC3, and TC4 sites using a PCR-based mutagenesis method.

The reporter vector pPL consisted of the *SV40* promoter and the *luciferase* gene and is identical to the pGL3-Promoter vector (Promega). pTPL, pAPL, and pBPL contained the *TNF* promoter (−1044 to +54 from the transcription start site), *LTα* promoter (−924 to +43 from the transcription start site), and *LTβ* promoter (−971 to +12 from the transcription start site), respectively, instead of the *SV40* promoter of pPL. TE1 and TE2 sequences were PCR amplified and inserted upstream of pPL, pTPL, pAPL, and pBPL (pTE1-PL, pTE2-PL, pTE1-TPL, pTE2-TPL, pTE2-APL, and pTE2-BPL). The primer sequences used to prepare the TE1 and the TE2 sequences were as follows: TE1-S, CCT GTG GCT GGA TGA AAT CT; TE1-AS, CCT GGG CAA CAA AGT GAG AC; TE2-S, CCA GGG GAG TTG TGT CTG TAA; TE2-AS, GCA GTT CGG TTC CTT GTT CT.

Reporter vectors (0.05 pmol) were transfected into Hep3B cells (1.0×10^5 cells) in a 12-well plate, using FuGene6 reagent (Roche Applied Science), and analyzed using a luciferase reporter assay system (Promega) after 24 h. For dual luciferase activities (26), values are shown as means and standard deviations of the results from at least three independent experiments.

qRT-PCR. Total RNA was isolated from cultured cells with TRIzol (Invitrogen). The cDNA synthesis used 2 μg of total RNAs that was reverse transcribed using a High Capacity cDNA reverse transcription kit (Applied Biosystems), according to the manufacturer's instructions. Quantitative PCR was performed using an ABI Prism 7300 system (Applied Biosystems) and SYBR green fluorescence. Each experiment was performed at least three times. The relative fold enrichment was quantified by normalization to *β-actin* or *glyceraldehyde-3-phosphate dehydrogenase* (*GAPDH*) gene expression. Primer sequences are listed in Table S1 in the supplemental material.

siRNA-mediated knockdown. Small interfering RNAs (siRNAs) for GL3, CTCF, and Rad21 were used as previously reported (40). RELA silencer select validated siRNA (s11914; Ambion) was used for p65 knockdown. siRNAs were transfected using the Lipofectamine RNAiMAX reagent (Invitrogen) for 48 h.

3C assay. For the chromosome conformation capture (3C) assays (21, 52), formaldehyde-cross-linked chromatin from Hep3B and NeHepLxHT cells was digested with DpnII overnight, followed by ligation with T4 DNA ligase at 16°C for 4 h. To prepare control templates for standard curves, a bacterial artificial chromosome spanning the *TNF/LT* locus RPCI11.C-47E16 was digested with Sau3AI, which is insensitive to Dam methylase, followed by random religation. After reversing the cross-links, genomic DNA was purified by phenol extraction and ethanol precipitation. The ligated products were assessed using qPCR with an ABI Prism 7300 system (Applied Biosystems) and Thunderbird SYBR qPCR Mix (Toyobo). The efficiency of DpnII digestion was evaluated after the entire 3C treatment using qPCR to amplify uncut fragments spanning the DpnII site. More than 80% of the individual restriction sites were digested in these experiments. The 3C-qPCR data were normalized to a loading control, using internal primers located in the *TNF/LT* gene locus. We gained similar results after normalization with internal primers located in *GAPDH* (data not shown). The relative frequencies of interactions between the reference and its physically close site in the control state were finally normalized to 1. Examples of the calculation for relative interacting frequencies are described in Results. Statistical analysis was performed using Student's *t* test for the results of more than three independent experiments. Primer sequences are listed in Table S1 in the supplemental material.

Immunofluorescence analysis. Cultured human cells were fixed with 4% paraformaldehyde in phosphate-buffered saline (PBS) for 10 min at room temperature. Fixed cells were rinsed three times in PBS for 5 min and permeabilized with PBS containing 0.2% Triton X-100 and 0.5% normal goat serum (NGS) for 5 min on ice. Cells were rinsed three times in PBS containing 0.5% NGS for 5 min and then incubated with rabbit anti-p65 (sc-372; Santa Cruz) for 60 min followed by secondary donkey Cy3-conjugated or Alexa Fluor 488-conjugated antibodies for 60 min. Labeled cells were washed three times in PBS for 10 min each. Samples were analyzed using a fluorescence microscope system (Orca-ER1394; Olympus).

Patients and histological assessment. A total of 38 patients (male, 29; female, 9) with HCC, who had undergone tumor resection at the National Cancer Center Hospital, Tokyo, Japan, between May 2003 and December 2005, were enrolled in the present study. The median patient age and follow-up period were 63 years and 1,719 days, respectively. Among the 38 HCC patients, 12 were immunologically positive for hepatitis C virus (HCV) infection, and 16 for persistent hepatitis B virus (HBV) infection (hepatitis B virus surface antigen positive), and 10 were negative for both HCV and HBV infection. Histological examination of noncancerous liver tissue samples revealed findings compatible with chronic hepatitis in 22 and cirrhosis in 9 and no remarkable histological findings in 7. The 38 HCCs were histologically classified into 3 well-differentiated, 27 moderately differentiated, and 8 poorly differentiated tumors. All patients were followed for more than 100 days. Clinical and pathological profiles were obtained from the medical records of the patients. This study was approved by the Ethics Committee of the National Cancer Center, Tokyo, Japan, and written informed consent was obtained from all patients.

IHC. Immunohistochemistry (IHC) for TNF and LTβ was performed using a polymer-based method with the Envision+Dual Link system-horseradish peroxidase [HRP] (DK-2600 Glostrup; Dako). Sources and dilutions of primary antibodies were as follows: anti-TNF-α (ab9579), 1:100, Abcam; anti-LTβ (ab64835), 1:50, Santa Cruz Biotechnology. Formalin-fixed, paraffin-embedded serial tissue sections (4 μm) were placed on silane-coated slides for IHC. Sections cut through the maximum tumor diameter were selected for IHC evaluation. The sections were deparaffinized and rehydrated in xylene and grade-diluted ethanol (50 to 100%) and submerged for 20 min in 0.3% hydrogen peroxide with absolute methanol to block endogenous peroxidase activity. Antigen retrieval for TNF and LTβ was carried out by heating in target retrieval solution (Tris-EDTA buffer, pH 9; Dako Cytomation) at 121°C for 10 min by a pressure cooker. After protein blocking, the sections were incubated with each primary antibody at room temperature for 1 h, followed by incubation with Envision+Dual Link reagent at room temperature for 30 min, and visualized using 3,3-diaminobenzidine tetrahydrochloride as a chromogen. Finally, the sections were counterstained with hematoxylin. Sections were gently rinsed in PBS between incubation steps. The primary antibody was omitted from the reaction sequence as a negative control.

All sections were evaluated by two pathologists, Y. Kanai and H. Ojima, with no knowledge of any clinical or pathological information. Immunoreactivities of TNF and LTβ were defined as follows: negative, no cytoplasmic staining was observed or the intensity of cytoplasmic staining was lower than that for noncancerous hepatocytes within the same section in more than 50% of cancer cells; positive, the intensity of cytoplasmic staining was equivalent to or higher than that of noncancerous hepatocytes in more than 50% of cancer cells.

Statistical analysis. Differences between groups were analyzed using Student's *t* test. A P value of <0.05 was considered statistically significant.

RESULTS

Distribution of CTCF-enriched sites in the human *TNF/LT* gene cluster. CTCF-enriched sites in the human *TNF/LT* gene region were investigated by checking several genome-wide CTCF-binding profiles available on websites and in our published data (40, 65). At least four CTCF-enriched sites (TC1, TC2, TC3, and TC4) were identified in this locus and were conserved among the cells tested (Fig. 1A; see also Fig. S1A in the supplemental material). There were no probe sets for the TC2 site in genome tiling arrays because of the presence of frequent repeat sequences (shown by asterisks in Fig. S1A in the supplemental material). Interestingly, TC3 was located between the *TNF* and *LTβ* gene promoters, forming the possible boundary between these adjacent chromosomal subregions.

Based on previous reports (28, 69), each TC site contained a 20-bp consensus CTCF-binding motif (Fig. 1B). To determine if CTCF bound directly to these TC sequences, we performed electrophoretic mobility shift assays (EMSAs) using radiolabeled duplex probes of approximately 100 bp for each TC site and the *in vitro* transcribed/translated CTCF protein. Similar to the DMR insulator of the *H19* gene used as a control (40), the TC probes formed complexes with CTCF and were further supershifted by anti-CTCF antibodies. In contrast, negative-control (NC) probes, which had sequences located downstream of the *NFKBIL1* gene, did not bind to CTCF. In addition, competition assays using mutated TC probes carrying base substitutions within the consensus motif showed that mutated probes did not bind to the CTCF protein (see Fig. S1B and C in the supplemental material), indicating that CTCF specifically bound to the TC sequences.

In order to clarify the localization of CTCF and the cofactor cohesin RAD21 in hepatic cells, we performed chromatin immunoprecipitation (ChIP) analyses using anti-CTCF and anti-RAD21 antibodies, followed by quantitative PCR (qPCR) (Fig. 1C and D). We used standard cell lines: Hep3B, which originates from human HCC, and NeHepLxHT, which is a telomerase-immortalized human neonatal hepatocyte line (51). Both CTCF and RAD21 bound to the TC sites but not to the NC site. RAD21 was relatively enriched with CTCF at TC1 in the *TNF/LT* locus. The CTCF enrichment at the TC sites in Hep3B cells may be remarkable due to the high expression of this gene (see Fig. S1D in the supplemental material) compared with that in NeHepLxHT cells.

Differential regulation of *TNF/LT* genes under TNF stimulation. To examine the transcriptional regulation of the *TNF/LT*

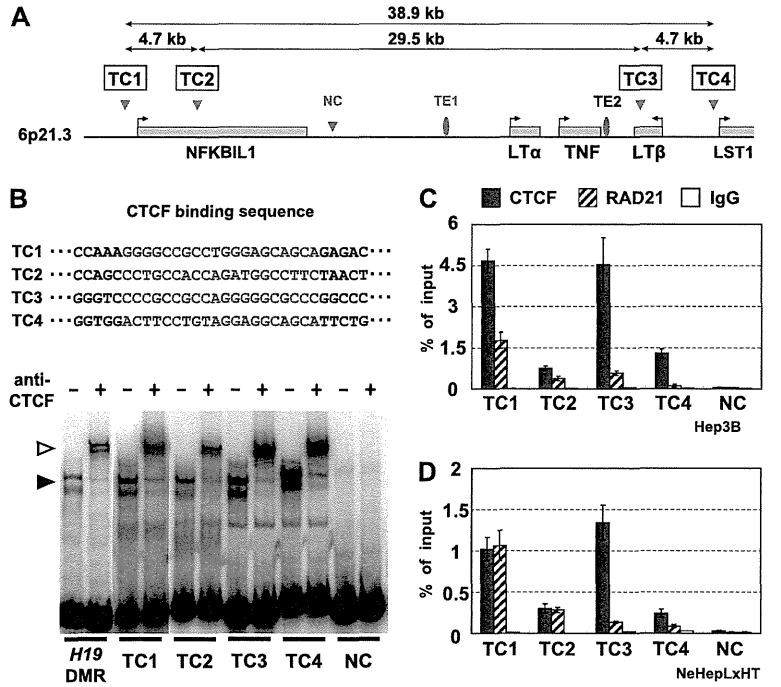

FIG 1 CTCF-enriched sites in the human *TNF/LT* gene cluster locus. (A) CTCF-enriched sites in the *TNF/LT* locus on human chromosome 6p21.3. In addition to the *NFKBIL1*, *LTα*, *TNF*, *LTβ*, and *LST1* genes, a newly identified TE2 enhancer is indicated by a red oval. Based on genome-wide CTCF-binding profiles available from websites and our published data (see Fig. S1A in the supplemental material), four enriched sites were designated TC1, TC2, TC3, and TC4. NC is used as a negative control, and TE1 is a site with no enhancer activity. (B) Direct binding of CTCF to TC sequences. Predicted CTCF-binding sequences within TC1, TC2, TC3, and TC4 sites are indicated, together with the 20-bp consensus motif (red). For EMSAs, radiolabeled duplex probes of approximately 100 bp for each TC site were incubated with anti-CTCF antibodies and synthesized CTCF. Solid and open arrowheads indicate CTCF DNA and the supershifted complexes, respectively. The *H19* DMR insulator and an intergenic unrelated sequence (NC) were used as controls. (C and D) Existence of CTCF and the cofactor cohesin RAD21 at TC sites. Chromatin immunoprecipitation analyses were carried out with anti-CTCF and anti-RAD21 antibodies and control IgG, followed by quantitative PCR with specific primers for each TC site in Hep3B cells (C) or NeHepLxHT cells (D).

genes, we performed quantitative reverse transcription (RT)-PCR (qRT-PCR) analyses with Hep3B and NeHepLxHT cells stimulated by TNF-induced NF-κB activation (Fig. 2A; see also Fig. S2A and B in the supplemental material). Expression of *LTα* and *TNF* mRNAs was markedly increased in Hep3B cells 1 h after stimulation, but *LTβ* mRNA was not simultaneously induced. Moreover, *TNF* expression seemed to be variable after the 1-h peak, while *LTα* and *LTβ* expression did not peak until 24 h after TNF treatment. Early induction of the *LTα* and *TNF* genes also occurred in NeHepLxHT cells, with subsequent expression of the *LTβ* gene. The patterns of *TNF/LT* expression differed between these cell lines, probably due to the constitutively low activation of the NF-κB pathway in Hep3B cells (see Fig. 4A) (11, 55).

Nuclear translocation of NF-κB is critical for its activation (24), and we therefore investigated its subcellular localization under TNF stimulation, using immunofluorescent staining of p65, a subunit of the NF-κB heterodimer (Fig. 2B; see also Fig. S2C in the supplemental material). Cytoplasmic p65 translocated to the nucleus at 30 min after stimulation, and this translocation was inhibited by the addition of BAY11-7082, a specific inhibitor of IκBα phosphorylation (48). The translocated p65 was found to decrease at 1 h after the stimulation (see Fig. S2D in the supplemental material). The expression status of the *TNF/LT* genes was analyzed in parallel using qRT-PCR analyses (Fig. 2C and D). TNF-induced expression of *TNF*, *LTα*, and *LTβ* was attenuated by NF-κB inhibition. Since the use of BAY11-7082 had cytotoxic effects at late time points after TNF stimulation, we carried out siRNA-mediated knockdown of p65 (see Fig. S2G and H in the supplemental material). The induction of the *TNF*, *LTα*, and *LTβ* genes was consistently inhibited by depletion of p65, indicating that the *TNF/LT* genes are regulated by NF-κB in the TNF-treated hepatic cells. Expression of the neighboring *NFKBIL1* gene was unaffected by the stimulation. TNF treatment caused no significant cell damage throughout the study (see Fig. S2E and F in the supplemental material). Thus, the *TNF/LT* genes are differentially induced by TNF-activated NF-κB signaling.

CTCF-dependent enhancer-blocking activity in the *TNF/LT* gene locus. Previous studies demonstrated that the *H19* DMR insulator contains multiple CTCF-binding sites, which are essential for enhancer-blocking activity (6, 22, 26). Luciferase reporter assays were performed with Hep3B cells to test the enhancer-blocking effects of TC1, TC2, TC3, and TC4 (Fig. 3). The presence of TC1, TC2, TC3, and TC4 between the enhancer and promoter reduced the luciferase activities to approximately 60% of those for the control pIHLE vector (pIHLTE-1F, pIHLTE-2F, pIHLTE-3F, and pIHLTE-4F). TC sequences in the opposite direction showed similar results (pIHLTE-1R, pIHLTE-2R, pIHLTE-3R, and pIHLTE-4R), indicating that the TC sites possess enhancer-block-

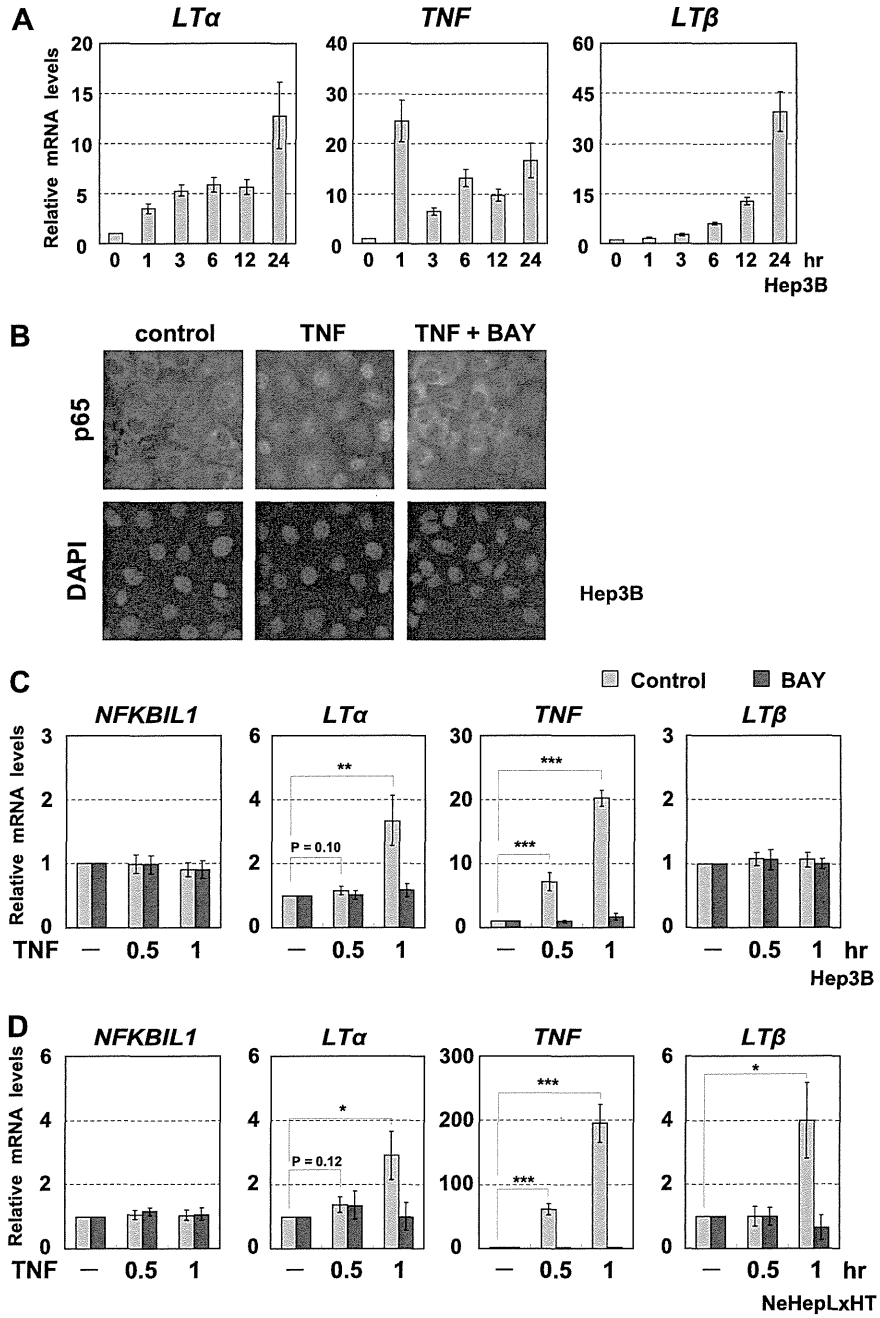

FIG 2 Differential regulation of *TNF/LT* genes under TNF stimulation. (A) Effect of TNF stimulation on *TNF/LT* expression in Hep3B cells. qRT-PCR analyses were performed with Hep3B cells under TNF treatment. (B) Nuclear translocation of NF-κB induced by TNF stimulation. The subcellular localization of the p65 subunit of the NF-κB heterodimer was analyzed by immunofluorescent staining of TNF-stimulated Hep3B cells, together with the use of BAY11-7082, an inhibitor of NF-κB activation. (C and D) NF-κB-dependent expression of the *TNF/LT* genes. TNF-induced expression of the *TNF/LT* genes was examined by qRT-PCR analyses in Hep3B (C) or NeHepLxHT (D) cells in combination with NF-κB inhibition. *, $P < 0.05$; **, $P < 0.01$; ***, $P < 0.005$.

ing activities that are independent of the orientation of the sequences. To exclude the possibility that the TC sites exhibit silencer-like activities, the TC sequences were placed downstream of the enhancer (pIHLET-1F, pIHLET-1R, pIHLET-2F, pIHLET-2R, pIHLET-3F, pIHLET-3R, pIHLET-4F, and pIHLET-4R). Luciferase activity was not reduced by TC sites in this position, suggesting that TC sites do not possess silencer-like functions. The use of mutant TC sites lacking CTCF-binding function, as described

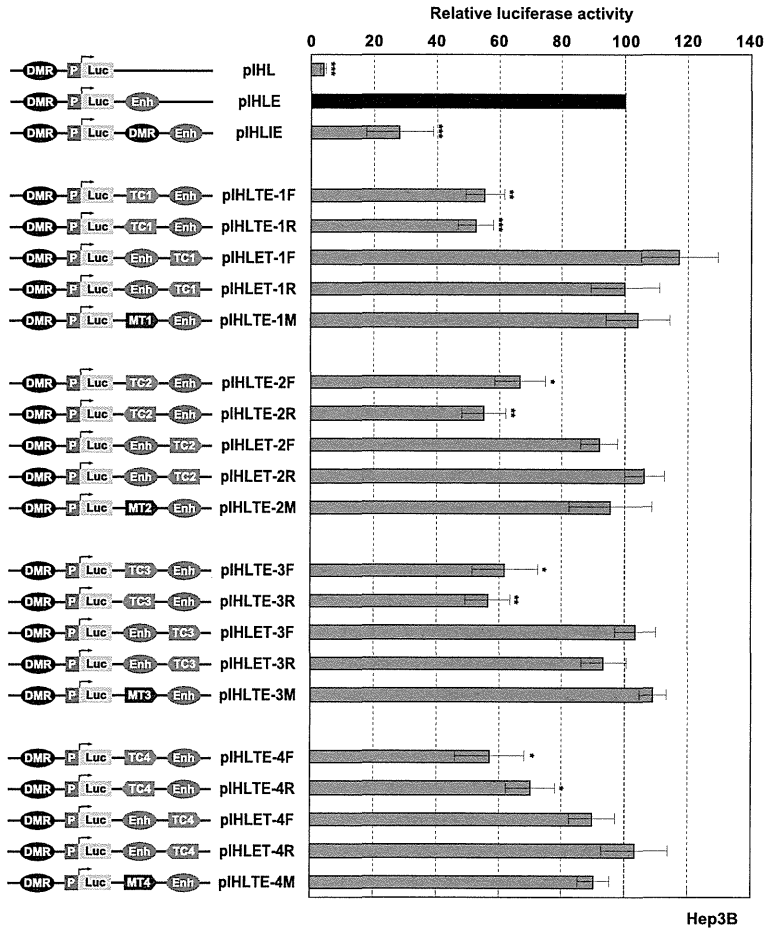

FIG 3 CTCF-dependent enhancer-blocking activity of TC sequences. pIHLTE plasmids were constructed by inserting fragments of approximately 200 bp containing wild-type or mutant-type TC (lacking the CTCF binding function) between the promoter and the enhancer in pIHLE. The *H19* DMR insulator was used as a control. For pIHLET, TC fragments were inserted downstream of the enhancer in pIHLE. The luciferase activities from pIHLE were normalized to 100. The values are given as means and standard deviations of the results from more than three independent experiments. Luc, *luciferase* gene; P, *H19* promoter; Enh, SV40 enhancer; DMR, *H19* DMR insulator; TC1-TC4, CTCF-enriched sites; MT1 to MT4, the mutant TC sequences. *, $P < 0.05$; **, $P < 0.01$; ***, $P < 0.005$.

above (see Fig. S1B and C in the supplemental material), demonstrated no enhancer-blocking effects (pIHLTE-1M, pIHLTE-2M, pIHLTE-3M, and pIHLTE-4M), further suggesting that the insulator activities of the TC sites depend on CTCF. These results suggest that TC1, TC2, TC3, and TC4 are functional insulators.

Characterization of a TNF-responsive hepatic enhancer in the human *TNF/LT* locus. In order to understand the overall regulatory mechanisms in the *TNF/LT* locus, we investigated the role of transcriptional enhancers in hepatic cells. Based on several DNase-hypersensitive sites in the locus (56), modified histones, p300 binding, previously reported enhancers (HSS-9 and HSS+3) in mouse T cells (58), and κB-responsive elements conserved among humans, mice, and rats (30, 31), we chose two candidates, named TE1 and TE2, which were located about 3.5 kb upstream of the *LTα* gene and just downstream of the *TNF* gene, respectively (Fig. 1A; see also Fig. S1A in the supplemental material). Luciferase reporter assays were performed with Hep3B cells to determine if TE1 and TE2 act as enhancers (Fig. 4A). Compared to the control (pPL) and TE1 (pTE1-PL), TE2 significantly increased transcription from the *SV40*, *TNF*, *LTα*, and *LTβ* promoters (pTE2-PL, pTE2-TPL, pTE2-APL, and pTE2-BPL), probably because of the constitutively low activation of NF-κB in Hep3B cells. Under TNF stimulation, these promoter activities were further elevated. These results indicate that TE2 has a TNF-responsive enhancing effect on the *TNF/LT* gene promoters. In addition, the effect of TE2 on the *LTα* promoter seemed to be weaker than that on the *TNF* promoter. The TNF-inducible enhancer activities of TE2 were also detected in other cell lines (see Fig. S3A in the supplemental material).

NF-κB p65 cooperates with histone acetyltransferase p300 (74), which functions as a transcriptional coactivator that accumulates in active enhancer elements (61). To validate the role of TE2 as an active enhancer, we investigated recruitment of p65 and p300 to TE2 by TNF stimulation in Hep3B cells, using ChIP-qPCR assays (Fig. 4B and C). A previously demonstrated enhancer of the *MCP-1* gene (ME) was used as a control (57). Recruitment of p65

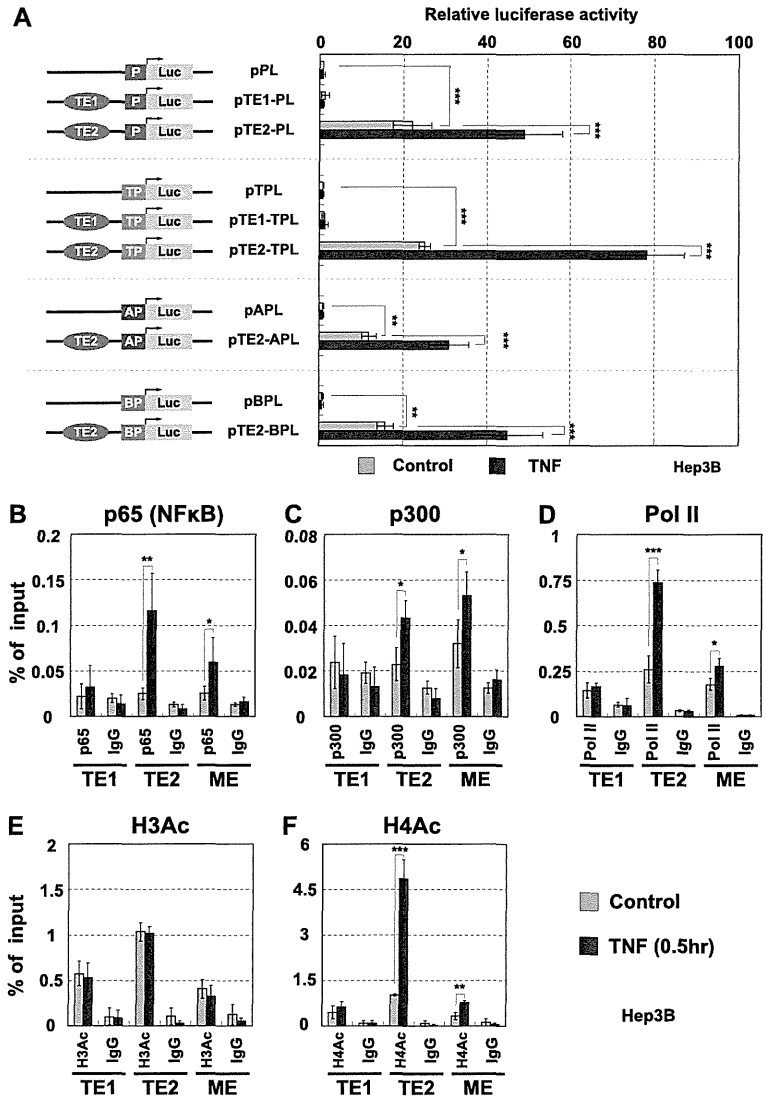

FIG 4 Characterization of TNF-responsive enhancer in the human *TNF/LT* locus. (A) Enhancer activity of TE2. The *luciferase* reporter vectors pPL, pTPL, pAPL, and pBPL contained the *SV40* promoter, *TNF* promoter, *LTα* promoter, and *LTβ* promoter, respectively. The candidate enhancers TE1 and TE2 were inserted in these vectors upstream of the promoter. Hep3B cells were transfected with the reporter vectors and treated with TNF for 3 h (solid bars). Luciferase activities were normalized to basal pPL, pTPL, pAPL, and pBPL. The values are given as means and standard deviations of the results from more than three independent experiments. P, SV40 promoter; TP, *TNF* promoter; AP, *LTα* promoter; BP, *LTβ* promoter. (B to E) The chromatin state of the TE2 enhancer in TNF-stimulated Hep3B cells. ChIP assays were performed with antibodies against p65/NF-κB (B), p300 (C), RNA polymerase II (D), or acetylated histone H3 (E) or H4 (F). The *MCP1* enhancer (ME) was used as a positive control. The values are given as means and standard deviations of the results from more than three independent experiments. *, $P < 0.05$; **, $P < 0.01$; ***, $P < 0.005$.

and p300 to TE2 occurred at 0.5 h after TNF stimulation. Interestingly, RNA polymerase II (Pol II) and acetylated histone H4 were also significantly enriched at TE2 (Fig. 4D to F). In contrast, histone H3 acetylation showed no remarkable changes (Fig. 4E). It was previously reported that various stimuli, such as serum, interleukin 1β (IL-1β), gamma interferon (IFN-γ), and TNF induced the acetylation of histone H4 but not histone H3 (2, 13, 32). Similar data were obtained in NeHepLxHT cells (see Fig. S3B in the supplemental material). These results indicate that TE2 is an active enhancer, which has four putative κB-binding motifs (see Fig. S3C in the supplemental material), under TNF-stimulated conditions in hepatic cells.

CTCF and the cofactor cohesin are involved in transcriptional regulation in the *TNF/LT* gene cluster. RNA interference-mediated knockdown in Hep3B cells was used to determine if CTCF and cohesin, which are enriched at the TC insulators, were involved in transcriptional regulation in the *TNF/LT* locus. Western blot and qRT-PCR analyses showed that CTCF and RAD21

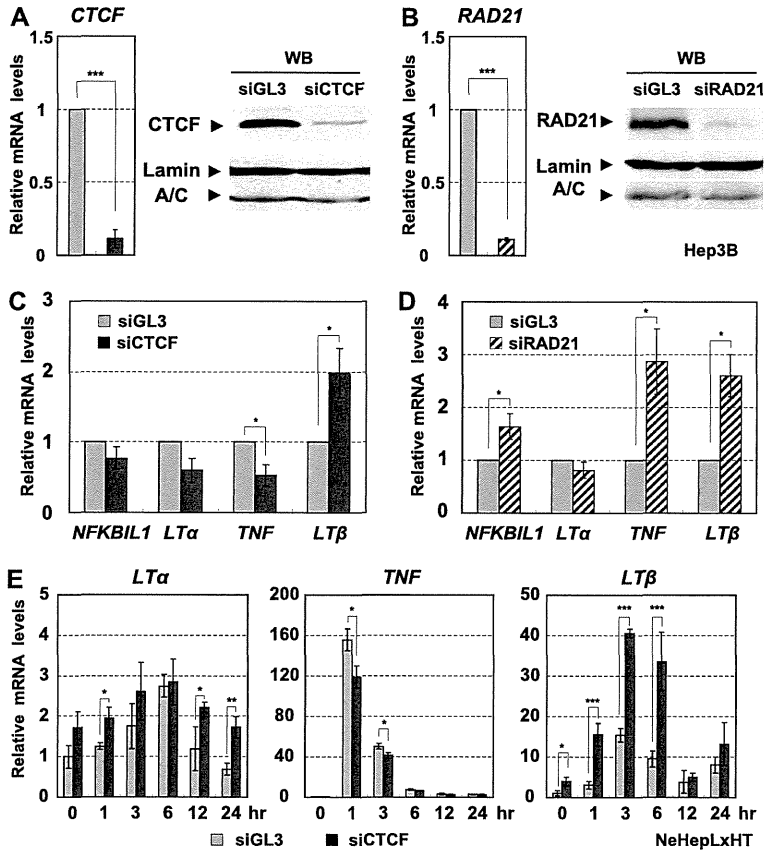

FIG 5 CTCF-mediated insulators are involved in transcriptional regulation in the *TNF/LT* gene cluster. (A and B) RNA interference-mediated knockdown of CTCF (A) and the cofactor cohesin RAD21 (B). Western blot and qRT-PCR analyses were carried out with Hep3B cells. As previously demonstrated (40), more than two distinct siRNAs against CTCF or RAD21 and control siRNAs were used in the experiments. (C and D) Effects of CTCF and RAD21 knockdown on the transcriptional status of the *TNF/LT* genes. Using qRT-PCR analyses, the transcriptional levels of these genes were analyzed relative to that of *β-actin* and were normalized with the control GL3. (E) Effect of CTCF knockdown on *TNF/LT* expression in TNF-stimulated NeHepLxHT cells. CTCF siRNAs were introduced into NeHepLxHT cells for 48 h, followed by TNF treatment for the indicated time period. Values are given as means and standard deviations of the results from more than three independent experiments. *, $P < 0.05$; **, $P < 0.01$; ***, $P < 0.005$.

were depleted at both the protein and RNA levels (Fig. 5A and B). ChIP-qPCR confirmed that the amounts of CTCF and RAD21 were significantly reduced at each TC site in the knockdown cells (see Fig. S4A and B in the supplemental material). The effect of the knockdown on the constitutively low activation of the *TNF/LT* genes in Hep3B cells was tested by qRT-PCR analyses (Fig. 5C and D). The loss of CTCF reduced *TNF* expression and increased *LTβ* expression, while RAD21 depletion increased *NFKBIL1*, *TNF*, and *LTβ* expression, suggesting that CTCF and cohesin have overlapping but certain distinct roles. Indeed, cohesin was reported to be able to behave as a transcriptional regulator, independent of CTCF (46, 54, 65).

We also analyzed the effects of CTCF knockdown on *TNF/LT* genes in TNF-treated NeHepLxHT cells in which the *TNF/LT* genes are normally silenced (Fig. 5E). The loss of CTCF reduced *TNF* expression and accelerated *LTβ* induction in the stimulated cells (Fig. 5E; see also Fig. S4C to 4E in the supplemental material). These results suggest that CTCF/cohesin-mediated insulators are involved in the transcriptional regulation of the *TNF/LT* gene cluster. It is notable, however, that TNF stimulation itself did not affect the degrees of CTCF and RAD21 enrichment at each TC site (see Fig. S4F and G in the supplemental material), suggesting that higher-order chromatin regulation may be involved in the expression of the *TNF/LT* genes upon TNF stimulation. We assessed the knockdown effects with no significant cell damage throughout the study (see Fig. S4H and I in the supplemental material).

Dynamics of higher-order chromatin conformation in the *TNF/LT* locus. 3C assays were performed with Hep3B and NeHepLxHT cells to investigate higher-order chromatin regulation in the *TNF/LT* locus, where TE2 enhancer, gene promoters and TC insulators were identified as functional elements (Fig. 6; see also Fig. S5 in the supplemental material). Use of the 4-bp-recognizing restriction enzyme DpnII allowed us to examine these elements separately. Based on qPCR analyses of the intramolecular ligation products, the relative interacting frequencies of the reference site (yellow bar) with other 7 DpnII fragments containing each element in the *TNF/LT* locus were measured, as further described in Fig. S6 in the supplemental material. TE2 and TC2 were mainly chosen as the reference sites because of their effectiveness in the experiments. The efficiency of DpnII digestion of

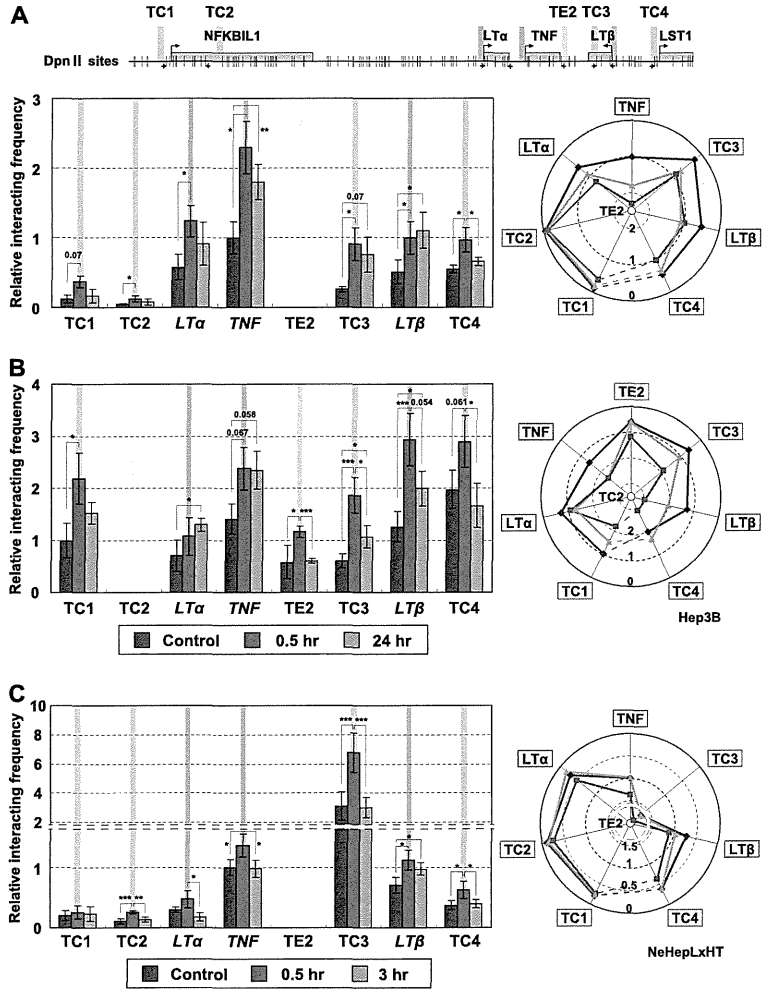

FIG 6 Dynamic changes in higher-order chromatin conformation of the *TNF/LT* locus under TNF stimulation. DpnII digestion was used to design 3C analyses to allow the examination of individual fragments containing each TC site, TNF/LT gene promoter, and TE2 enhancer. (A) The relative interacting frequencies between the reference TE2 fragment (yellow bar) and other DpnII fragments were determined by qPCR analyses of at least three distinct samples from Hep3B cells under TNF treatment. The relative frequencies of interactions between the reference TC2 (yellow bar) and other DpnII fragments in Hep3B cells (B) or between the reference TE2 (yellow bar) and other DpnII fragments in NeHepLxHT cells (C) are shown. In the right panel, the radar chart shows the average relative frequencies of interactions between the reference (central yellow circle) and each functional element. PCR amplification using internal primers located in the *TNF/LT* locus was used for a loading control to normalize the amount of DNA fragments. Efficiencies of DpnII digestion and subsequent ligation were confirmed at each restriction site used. The relative frequencies of interactions between the reference and its physically close site in the control state were normalized to 1 (TE2-*TNF* [A and C] or TC2-TC1 [B]). Control basal state, blue; *TNF*-expressing state, magenta; *TNF/LTβ*-expressing state, green. TC sites, *TNF/LT* gene promoters, and TE2 enhancer are indicated by the same color bars in the locus (upper panel) and the 3C data. The values are given as means and standard deviations of the results from more than three independent experiments. *, $P < 0.05$; **, $P < 0.01$; ***, $P < 0.005$.

individual sites was > 80%, and samples without ligation gave no PCR-amplified products. We determined if CTCF knockdown affected the chromatin conformation of the *TNF/LT* locus in Hep3B cells (see Fig. S5A and B in the supplemental material). Compared with the basal control state, the frequencies of interactions of the referenced TE2 or TC2 with other fragments were mostly reduced to <50% in the CTCF-depleted cells, suggesting that CTCF is involved in the basal conformation of the locus.

To clarify the spatiotemporal chromatin dynamics of the *TNF/LT* locus, we then examined the frequencies of interaction between these regulatory elements under TNF stimulation (Fig. 6). 3C assays were carried out in the cells under the basal control state, *TNF*-expressing state (0.5 h after stimulation), and *TNF/LTβ*-expressing state (24 or 3 h after stimulation). Compared with results for the basal control state, the frequencies of TE2 interaction with other sites tested in the locus were significantly augmented in *TNF*-expressing Hep3B cells (Fig. 6A), suggesting that intrachromosomal interaction occurred in the locus. Interestingly, TE2 maintained an interaction with the *LTβ* promoter and TC3 in the *TNF/LTβ*-expressing state while remaining separate

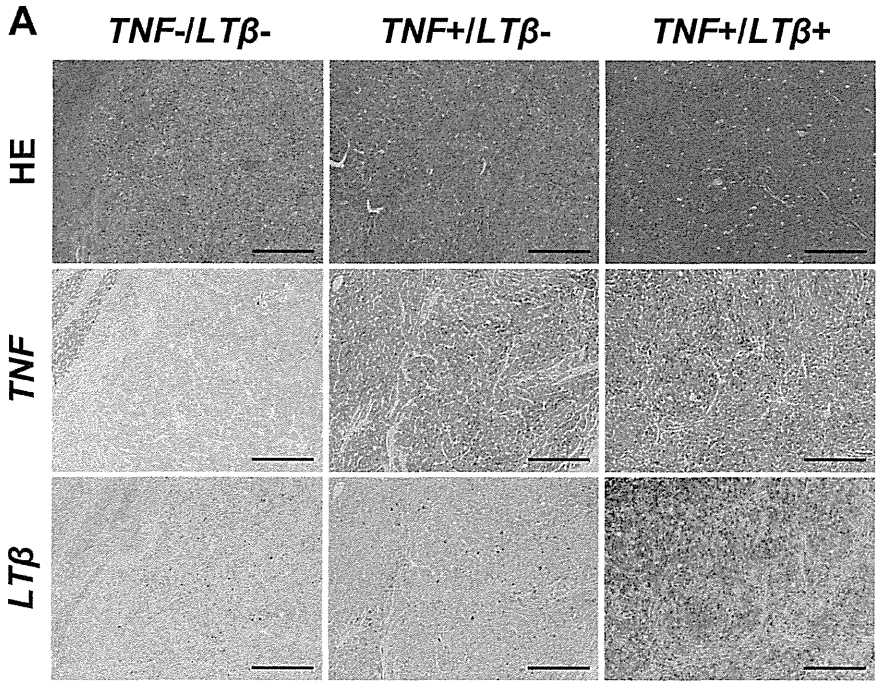

B

TNF \ LTβ	+	-
+	12/38 (31.6 %)	10/38 (26.3 %)
-	0/38 (0 %)	16/38 (42.1 %)

FIG 7 Expression of TNF and LTβ in human hepatocellular carcinoma tissues. (A) Representative immunohistochemical staining of human HCC. When the intensity of cytoplasmic staining was equivalent to or higher than that for noncancerous hepatocytes in >50% of cancer cells, the case was defined as positively stained. Three representative cases of the 38 cancer tissue samples tested are shown. Hematoxylin-and-eosin staining (upper) and immunostaining for TNF (middle) and LTβ (lower) are shown. Scale bar, 500 μm. (B) Percentages of TNF- and LTβ-stained cancer tissues. Cases with neither TNF nor LTβ expression (TNF− LTβ−), expression of both (TNF+ LTβ+), and TNF expression alone (TNF+ LTβ−) were found in 42.1%, 31.6%, and 26.3% of the cancer tissues, respectively. No cases expressed LTβ alone. The data for each tissue are summarized in Table S2 in the supplemental material.

from other elements. We also examined the frequencies of TC2 ligation with other fragments and found that TC2 enhanced the interaction with other fragments in the *TNF*-expressing state (Fig. 6B). However, TC2 maintained its close localization with the *TNF* and *LTα* promoters, but not with other fragments, in the *TNF/LTβ*-expressing state. Using the TE2 fragment as a reference, similar data were obtained in TNF-stimulated NeHepLxHT cells (Fig. 6C), except for some interactions of TE2 with the TC3, TC1, and *LTα* promoter. Using the TC2 fragment as a reference, we did not clearly detect the interactions with other fragments in NeHepLxHT cells. Collectively, these data suggest that the enhancer-promoter interactions are selectively controlled by intrachromosomal association and subsequent dissociation of the *TNF/LT* locus upon activation of TNF signaling. To further demonstrate interactions between TC insulators in chromatin reorganization, we assessed their relative frequencies of interaction in these cells using TC4 as a reference (see Fig. S5C and D in the supplemental material). These TC sites consistently showed association in the *TNF*-expressing state and subsequent dissociation in the *TNF/LTβ*-expressing state (modeled in Fig. S7 in the supplemental material).

Expression of TNF and LTβ in human HCC tissues. To examine whether the expression of TNF and LTβ is differentially regulated *in vivo*, we carried out immunohistochemical (IHC) analyses of HCC tissues (Fig. 7). Immunoreactivities of TNF and LTβ were assessed by comparison with the intensity of cytoplasmic staining of noncancerous hepatocytes within the same section. Representative images are shown in Fig. 7A, and the data for each tissue are summarized in Table S2 in the supplemental material. As summarized in Fig. 7B, neither TNF nor LTβ expression was detected in 16 out of 38 HCCs studied (42.1%), while both were densely stained in 31.6% of the cancer tissues. Interestingly,